

OCT 16 1952



NATIONAL ADVISORY COMMITTEE FOR AERONAUTICS

TECHNICAL NOTE 2803

A THEORETICAL AND EXPERIMENTAL INVESTIGATION OF THE
INFLUENCE OF TEMPERATURE GRADIENTS ON THE
DEFORMATION AND BURST SPEEDS
OF ROTATING DISKS

By P. I. Wilterdink, A. G. Holms, and S. S. Manson

Lewis Flight Propulsion Laboratory
Cleveland, Ohio



Washington
October 1952

NACA LIBRARY
LANGLEY AERONAUTICAL LABORATORY
Langley Field, Va.

TECHNICAL NOTE 2803

A THEORETICAL AND EXPERIMENTAL INVESTIGATION OF THE INFLUENCE OF
TEMPERATURE GRADIENTS ON THE DEFORMATION AND BURST
SPEEDS OF ROTATING DISKS

By P. I. Wilterdink, A. G. Holms, and S. S. Manson

SUMMARY

The purposes of this investigation were to evaluate the influence of temperature gradients and to test the validity of a recently developed method of calculating plastic flow in disks by comparing calculated results with experimental observations.

Short-time spin tests on parallel-sided, 10-inch-diameter disks were conducted under conditions that subjected the disks to a range of temperatures from 70° to 1440° F and to a range of temperature differences between the rim and center from 0° to 1290° F. Measured plastic strains and experimental burst speeds were compared with the strains and burst speeds calculated from the short-time tensile properties of the disk material.

The agreement between the theoretical and experimental results was good over the wide range of temperature conditions investigated. Thermal gradients produced little reduction in burst speed of the disks which had high ductility; however, these gradients had a strong influence on the behavior of the disk during the early stages of plastic flow. The loss in tensile properties of the material, caused by the temperature of the material, had a greater effect in reducing the burst speed than the stresses set up by the thermal gradient.

INTRODUCTION

In turbojet and turbine-propeller engines, the turbine disk is one of the heaviest components, and it is also one of the components which uses a large amount of strategic material. Accurate knowledge of the factors that affect the strength of this part is needed to design turbine disks which will utilize the material in the disk most efficiently. The

rim of an aircraft-gas-turbine wheel operates at higher temperatures than the central portion of the disk. This condition may introduce thermal stresses of considerable magnitude. Because stress distributions in turbine disks are complex, many disks have been designed using rather large safety factors. If the stresses in the disk could be computed more accurately and the significance of these stresses could be determined experimentally, then disks could be designed less conservatively.

Because the rim of a turbine rotor operates at elevated temperatures, the materials in common use are subject to time-dependent phenomena similar to the creep and stress rupture that occur in elevated-temperature-material tests. Furthermore, the influence of thermal stresses accompanying temperature cycling can be an important cause of rim cracking in the case of some types of wheels with welded blades (reference 1). In contrast to the rim, the central portions of an aircraft-gas-turbine rotor generally operate at temperatures low enough so that the short-time properties of the material can be expected to correlate with flow and fracture phenomena involving the central region. Because the present investigation involved short-time tests and center failures, the results are regarded as being relevant to failures that might originate in a gas-turbine disk center, but the results do not apply to failures involving temperature cycling or time-dependent phenomena in the rim.

The purposes of the present investigation are to evaluate the significance of temperature distribution with respect to plastic deformations and center failures and to test the validity of a method (reference 2) of calculating plastic flow and fracture for rotating disks with temperature gradients.

Spin tests were performed on parallel-sided disks at room temperature and on disks that were subjected to center temperatures from 70° to 900° F and rim temperatures from 70° to 1440° F. An experimental analysis of the plastic strain distributions is compared with calculated strains, and experimental burst speeds are compared with calculated burst speeds. Comparison of calculated diameter changes and burst speeds with experimental diameter changes and burst speeds in reference 2 showed that the method of calculation was equally valid for parallel-sided and tapered disks under room temperature conditions. Although only parallel-sided disks were used in the present investigation, it is reasonable to expect that in the presence of temperature gradients, the method of calculation would be equally valid for thin tapered disks subject to center failures. All the work was performed at the NACA Lewis laboratory.

APPARATUS AND PROCEDURE

The disks were tested with the equipment shown in figure 1. In the test made at room temperature, the slip rings, induction heating coils, and cooling jet were not used.

2412

The rotational speed of the disks was measured with two electronic frequency meters, and the average of the two frequency-meter readings was used to compute the speed reported for each test. The only exception to this procedure occurred in the tests of three disks for which reliable readings were obtained from only one frequency meter at the burst speed. For the tests below the burst speed of the disk, the average difference in the two frequency meter readings was 0.5 percent. For the disk burst speed, the average difference in the two frequency-meter readings was 1.3 percent.

In the temperature-gradient tests, the temperatures were controlled by varying the amount of power supplied to the heating coil by the 10,000-cycle alternating-current supply and the use of the water cooling jet.

The temperatures were measured by chromel-alumel thermocouples which were installed as shown in figure 2. The thermocouples were spot-welded to the upper surface of the disk, and steel tubing with a cap at the outer end was used to protect the thermocouple wires. The thermocouple wires were brought to the slip rings through the hollow drive shaft on the disk. The details of the thermocouple slip rings are discussed in reference 3. No indications that the method used to install the thermocouples produced any loss of strength of the disks were observed. During the tests for which the rim temperatures were above 1400° F an optical pyrometer was used, and the readings obtained checked the thermocouple readings within the accuracy of the optical pyrometer (+12° F). The observer with the optical pyrometer was approximately 11 feet from the glass observation window in the evacuated test chamber (fig. 1), and a tube connecting the observation window and optical pyrometer was used to prevent extraneous light from interfering with the view of the test disk. The temperature distribution curves shown in figure 3 were based on an average of the thermocouple readings for all the disks tested under a given temperature-gradient condition.

The dimensions of the disks used in this investigation are shown in figure 4. The disk hub was reduced to 0.26-inch diameter adjacent to the disk so that the hub would have a minimum strengthening effect on the disk. Disks were inspected for defects by radiographic, Zyglo, and visual inspection methods. Inconel X was chosen as the disk material because it is age-hardenable and hence more uniform short-time properties can be expected than from hot-cold worked or quenched and tempered materials. The disks were made from bar stock by up-set forging. The heat-treating and forging practices were those recommended in reference 4. The heat treatment of the disks produced fully aged material, and a tensile specimen from the center of the disk had a ductility of 19.4 percent (reduction in area).

Disk growth measurements were made with conventional measuring equipment to the nearest 0.0001 inch after the disks were tested at speeds below 40,000 rpm and to the nearest 0.001 inch after they were tested at speeds above 40,000 rpm. The locations of the stations at which measurements used to compute strains were made are shown in figure 5. The change in radius and the change in thickness after each test was determined at each of the 10 stations. There were two stations separated by 90° for each radius, and the average change in dimensions at a given radius was used in the strain-distribution calculations. No evidence that these disks became elliptical or out of round as growth occurred was found.

The tensile specimens shown in figure 6 were cut from disks produced in a manner identical to the disks which were tested. Specimens were taken in the radial direction of the disks, and the minimum diameter of the specimen was located approximately $1\frac{7}{8}$ inches from the rim of the disk. The longitudinal axes of the specimens were in the center plane of the disks. One of the room-temperature specimens was taken from a disk and the minimum section of the specimen was in the center of the disk. Strains were obtained by measuring the change in diameter at the minimum section of the specimen.

The room-temperature tests were conducted by increasing the disk speed at a uniform rate until the desired speed was reached. Approximately 10 minutes was required to bring the disk up to the burst speed. In testing the disks with heated rims, the temperature and speed were increased simultaneously. Under these conditions, the time required to reach the burst speed was approximately 25 minutes.

PLASTIC FLOW AT ROOM TEMPERATURE

Change in Disk Diameter

The experimental points shown in figure 7 were obtained by measuring the diameter of the disk after it had been spun at speeds corresponding to the speeds shown by the ordinate. Since the diameter measurements were made on the disks in the nonrotating condition, the abscissa represents the change in diameter of the disk after the test was completed. All the experimental points were obtained from measurement of one test disk.

The agreement between the experimental measurements and the calculated curve in figure 7 is good up to the highest speed for which experimental measurements were available, and this speed was 2.1 percent below the burst speed of the test disk. The part of the theoretical curve extending beyond the last experimental point is discussed in the burst-speed section of this report.

Strain Distribution

The experimental points in figures 8 and 9 represent the conditions in the disk after rotation has stopped. The speed shown for each curve is the maximum speed reached during the test. At the lower plastic strains, the experimental strains at the center of the disk are slightly higher than the theoretical values. This trend is strongest for the changes in thickness shown in figure 8. The experimental points lie on or near the calculated curves in both figures 8 and 9.

The change-in-diameter curve (fig. 7) was calculated from the tangential strain at the rim. The theoretical and experimental tangential strains at the rim are in good agreement, as shown in figure 9, and correspondingly the experimental and theoretical change-in-diameter results of figure 7 are in good agreement.

The experimental disk burst at 43,800 rpm; it was not possible to obtain measurements for the radial and tangential strain distribution from the broken pieces, but the change-in-thickness measurements are presented in figure 10. The theoretical curve in figure 10 represents the change in thickness of the disks after operation at 43,800 rpm provided no failure occurs. This curve was calculated in the same manner as the curves presented in figure 8. The change in thickness at the rim obtained from the broken pieces was greater than that indicated by the theoretical curve. As confirmed by the shapes of the disk fragments in reference 5, the fracture is assumed to start in the highly stressed central region. After a crack has started in the center, the conditions of the theoretical calculation would no longer apply but the rim of the disk would continue to stretch which accounts for the fact that the experimental points of figure 10 lie above the calculated curve.

The theoretical curves (figs. 7 to 9) show that good agreement between calculations and experimental results were obtained over the entire range of speed from the onset of plastic flow to speeds quite close to failure. In particular, good agreement was achieved at 42,900 rpm for a disk that was subsequently burst at 43,800 rpm. The fact that the experimental points of figure 10 agreed with calculated results in the center of the disk (region of start of failure) suggests that the method of calculation is valid at all speeds up to the speed at which fracture starts.

Determination of Experimental Strain Distribution

The measured change in radius u at each station was converted into conventional tangential strain e_t by means of equation (1) (reference 6).

$$e_t = u/r \quad (1)$$

where r is the radius at the given station. (All symbols are defined in the appendix.) Since the thickness strain was available from thickness measurements, the radial strain was obtained from equation (2) after the usual assumption of no change in volume (reference 7) had been made.

$$\epsilon_r = - \epsilon_h - \epsilon_t \quad (2)$$

where ϵ_r , ϵ_h , and ϵ_t are the logarithmic strains in the radial, thickness, and tangential directions, respectively, at the given station. For plotting figure 9, ϵ_r was converted into conventional strain e_r .

There are other methods, of course, for determining the radial strain in the disk. The radial strain halfway between two points of measurement can be obtained from equation (3).

$$\frac{e_{r,n} + e_{r,n-1}}{2} = \frac{u_n - u_{n-1}}{r_n - r_{n-1}} \quad (3)$$

The radial strain can also be obtained from equation (4) (reference 6).

$$e_r = du/dr \quad (4)$$

Equations (3) and (4) were applied to the experimental measurements, giving results which were inferior to those obtained by the method of the preceding paragraph. The results with equations (3) and (4) were anticipated in view of the relatively large distances (fig. 5) between the points where the change in radius was measured.

Calculation of Theoretical Results

The stress-strain curves and the modulus of elasticity influence the theoretical results shown in figures 7 to 10 because the theoretical calculations (reference 2) were based on these factors. The stress-strain curves for the disk material are shown in figure 11, and the modulus of elasticity was obtained from reference 8.

The room-temperature ductilities determined from a rim specimen and from a center specimen were 20.7 and 19.4 percent reduction in area, respectively. The change-in-diameter measurements made on the tensile specimen were used to calculate the logarithmic longitudinal strain in figure 11 with the assumption that no change in volume occurred.

24/2 Although the ductility was higher in the rim of the disk than in the center (0.262 and 0.216 logarithmic longitudinal strain, respectively), the stress-strain curves of the center and rim specimens were otherwise identical. Because the highest strains are in the center of the disk, only the stress-strain curve (fig. 11) corresponding to the center specimen was used in the room-temperature calculations. The gage used to measure the change in diameter was not sensitive enough to determine the elastic portion of the curve; this portion of the curve was therefore drawn at a slope corresponding to the value of the modulus of elasticity obtained from reference 8.

The theoretical stresses and strains existing in the disk while it is rotating at a given speed were obtained by the method of reference 2, and the theoretical strains were corrected for unloading to obtain the conditions existing in the disk after rotation by the methods discussed in the latter part of the section entitled "Calculation of Theoretical Stress and Strain".

PLASTIC FLOW UNDER TEMPERATURE-GRADIENT CONDITIONS

Change in Disk Diameter

The experimental and theoretical results for the 90° F center, 880° F rim temperature-gradient tests are shown in figure 12. The temperature-distribution curve for both the theoretical calculations (solid line curve) and the experimental conditions is shown by curve A in figure 3. The experimental points in figure 12 were obtained by measurement of the diameter of the disk after it had been spun at speeds corresponding to those shown by the ordinate, and the abscissa represents the diameter of the disk after the test was completed or in the non-rotating condition. The experimental points were obtained with four disks corresponding to the data points indicated in figure 12.

The experimental points from the four disks fell on the same curve; that is, deformations for the same speed were very close together. For most disk materials there is usually a certain amount of variation in the properties from disk to disk; however, figure 12 shows that the short-time change in diameter behavior of the experimental disks of this age-hardenable material was quite uniform. The agreement between the experimental measurements and the calculated curve for the temperature-gradient conditions is good up to the highest speed for which experimental points are available in figure 12. The part of the theoretical curve extending beyond the last experimental point is discussed in the burst-speed section of the report.

Influence of the Temperature Gradient

The upper curve in figure 12, which is shown by the dashed line, is the theoretical curve for room-temperature conditions, and it was shown to be in good agreement with experimental results (fig. 7). The lower curve is the theoretical curve for the 90° F center, 880° F rim temperature conditions. The theoretical calculations show that the room-temperature disks should yield at 31,000 rpm and that the temperature-gradient disks having essentially the same center temperature should yield at 22,200 rpm. The experimental points obtained from the test disks confirm that yielding starts earlier in the temperature-gradient disk; the agreement of the experimental points with the theoretical curve indicates that plastic flow starts when the sum of the thermal and centrifugal stresses is equal to the yield point of the material. Both the theoretical curve and the experimental points show that the temperature-gradient disks stretch more than the room-temperature disks and that the greatest difference in the behavior of these disks occurs during the early stage of plastic flow.

The manner in which the stress distribution changes as the speed is increased is shown in figure 13. The greatest effect is shown by the tangential stresses; therefore, the radial stresses were not shown. The differences between the sets of curves is the result of both thermal expansion and differences in tensile properties. The greatest difference in stress distribution occurs at low speed, and as plastic flow takes place, the stress distributions approach each other (fig. 13). In both figures 12 and 13 it is shown that thermal gradients produce a strong influence on the disks during the early stages of plastic flow.

In the plastic range, the manner in which the thermal and centrifugal effects combine is, to a limited extent, similar to the elastic range. In the elastic stress range the combined effects of thermal expansion and centrifugal force can be obtained by calculating the stresses separately and then adding the two stress systems. The thermal expansion produces a force system which is in equilibrium; that is, the resultant of the tensile-stress distribution in the central part of the disk balances the resultant of the compressive stresses in the outer part of the disk, for a disk with a cold center and a hot rim. In such a balanced internal stress system, a reduction of the magnitude of stresses in one part of the system will automatically reduce the stresses in the other parts of the system. In the disk the centrifugal stresses, which are the result of externally applied forces, increase as the speed is increased.

In the plastic range, stress is not directly proportional to strain and the total stress in the disk cannot be obtained by adding stresses calculated for centrifugal forces only to stress calculated for thermal expansion only. At the higher speeds (plastic range), the slope of the

2412 stress-strain curve is much smaller than in the elastic range, and the change in stress accompanying a given amount of expansion is much less than that which occurs in the elastic range. Therefore, the application of a thermal gradient to a disk operating in the plastic range will produce a smaller change in the stresses in the disk than that which the same gradient would produce if it were applied to a disk operating in the elastic stress range. The relative positions of the maximum strains produced by the centrifugal forces and the thermal gradient influence the final strain distribution in the disk. The strain distributions resulting from the action of centrifugal forces are presented in figure 9, and it is evident that more plastic flow and expansion occurred in the center of the disk than in the outer part of the disk. In the case for which the thermal expansion of the outer part of the disk is greater than that in the center, the addition of thermal strains to a strain distribution of the type shown in figure 9 would not greatly increase the strains at the center of the disk (the critical region). Thus, the combined action of the decreasing slope of the stress-strain curve and the nature of the strain distributions produced by the centrifugal and thermal effects tends to reduce the importance of thermal stresses as plastic flow progresses in the disk.

For a disk of very low ductility, little plastic flow occurs and the thermal stresses could be important in raising the stresses to the level required for failure. For any material, the preceding discussions consider only the short-time properties of the material; the significance of thermal stress on the time-dependent behavior of the disk is considered outside the scope of the present investigation.

Strain Distribution

A comparison between the measured and theoretical strain distribution after the 90° F center, 880° F rim test is presented in figures 14 and 15. The solid-line curves were calculated by the same method as that used for the curves in figures 8 to 10. The agreement between the theoretical and measured results in figures 14 and 15 is good, and it is the same type of agreement as that obtained after the room-temperature test in figures 8 and 9. On the basis of the comparison between the theoretical curves and the experimental points for the room-temperature and the temperature-gradient tests, the introduction of the thermal gradient did not result in a loss in the accuracy of the calculations by the method of reference 2. The theoretical strains at the center of the temperature-gradient disk after the 43,000 rpm test, are 15 to 20 percent higher than those for the room-temperature disk after the 42,900 rpm test; the theoretical strains at the rim of the temperature-gradient disk are 30 to 40 percent higher than those for the room-temperature disk.

Calculation of Theoretical Stress and Strain

In the calculations by the method of reference 2 for the temperature-gradient conditions, the modulus of elasticity curve and the coefficient of thermal expansion curve in figure 16 were used, in addition to the stress-strain curves in figure 11. The stress-strain curves for the temperatures above room temperature were obtained from one radial-rim specimen for each temperature. For the calculations on a disk with a 900° F center, a stress-strain curve was interpolated between the 700° F curve and the 1000° F curve obtained from rim specimens, and the fracture strain was reduced by the same percentage as that observed for the loss in ductility between the rim and center specimens at room temperature.

The two sets of theoretical curves presented in figures 14 and 15 correspond to two methods of calculating the strains occurring during the unloading cycle (returning the disk to 0 rpm and room temperature). The broken-line set of strain distribution curves was obtained by considering the plastic flow which occurs during the unloading cycle.

In both the loading cycle (bringing the disk temperature and speed up to the 43,000 rpm conditions) and the unloading cycle, the assumption was made that the process was not dependent upon the path (manner in which speed and temperature are increased or decreased with respect to time) to an extent large enough to influence the results appreciably. In view of the agreement between the theoretical and experimental results in figures 14 and 15, the assumption of independence of the loading paths was reasonable. The exact nature and extent of dependence of stress-strain curves on the loading path has not, as yet, been established. For example, references 9 and 10 present conflicting evidence on the subject of loading paths.

If the stress-strain curve does not depend on the loading path, the stress-strain curves shown in figure 11 can be used in the method of reference 2 to compute the stresses and strains at any point of the loading or unloading cycle. For the purpose of illustrating the use of the stress-strain curves, a room-temperature stress-strain curve and a stress-strain curve for a high temperature H are presented in figure 17. When the disk was operating at 43,000 rpm speed and temperature conditions, point A represented the stress-strain condition computed by the method of reference 2 at the disk station which had a temperature H , and the permanent part of the total strain at point A on the stress-strain curve was Δ_1 . After the disk reached room temperature at the end of the test, Δ_1 was considered as the amount of permanent strain resulting from plastic flow during the loading cycle at the chosen station in the disk, and the new stress-strain curve (BDE) was used in the method of reference 2 to compute the stress and strains in the disk

after unloading. In the calculations corresponding to the nonrotating room-temperature conditions, the $\rho\omega^2$ and $\alpha\Delta T$ terms were set equal to zero. Point C represents the case in which the computed equivalent stress and strain after unloading is in the elastic range, and the total equivalent strain at the chosen station is $\Delta_1 + \Delta_2$. If the equivalent stress and strain corresponds to point F, plastic flow corresponding to DF occurred during the unloading, and the total equivalent strain remaining in the disk after unloading is $\Delta_1 + \Delta_3$. The dotted line curves in figure 16 were computed from the total equivalent strain remaining in the disk after unloading.

The equivalent stress distribution during the 43,000 rpm speed and temperature conditions is shown by the upper curve of figure 18 and the stress distribution after unloading is shown by the three lower curves. Beyond a disk radius of 4 inches, the calculations showed that a small amount of plastic flow occurred during the unloading cycle.

The solid-line set of strain distribution curves in figures 14 and 15 were calculated with the assumption that the unloading process was elastic. These curves differ only slightly from the curves which were based on plastic-flow calculations. In the cases where plastic flow occurred during the unloading cycle, the amount was thought to be small enough to be neglected, and the shorter method, in which elastic unloading was assumed, was used to obtain all the other calculated results. In the elastic unloading method for the room-temperature conditions, the strains obtained from the elastic stress calculations for a given speed were subtracted from the strains computed by the method of reference 2 at the same speed to obtain the strain distribution remaining in the disk after rotation. For the temperature-gradient conditions, the strains obtained from the calculated elastic stress distribution produced by the thermal gradient and the elastic centrifugal strains were subtracted from the strains computed by the method of reference 2 to obtain the strains remaining after rotation.

The change in disk thickness was computed from the strains remaining after rotation or permanent strains. The computations were made with the assumption that there was no change in volume.

The theoretical permanent change in disk diameter was obtained with equations (1) and (5).

$$e_t = u/r \quad (1)$$

$$\Delta D = 2u_b = 2r_b e_{t,b} \quad (5)$$

ΔD is the change in diameter; r_b is the radius of the outer edge of the disk, and $e_{t,b}$ is the theoretical permanent conventional tangential strain at the outer edge of the disk after the disk has been spun at a given speed.

INFLUENCE OF THERMAL GRADIENT AND MATERIAL PROPERTIES ON BURST SPEEDS

The Disk-Failure Process

A disk may fail by an instability process (that is, the speed passes through a maximum) or it may fail when the stresses and strains in the disk exceed the strength of the disk material. In reference 2 it was stated that generally it has been found that the strains accompanying burst are less than those required to cause instability and that apparently fracture is initiated under biaxial stress conditions before the high strains associated with instability can be induced. Theoretical calculations for the disks of the design and material used in this investigation showed that the ductility of the material was not of the very high order required to permit the occurrence of instability.

When the stresses in a disk are computed by the method of reference 2, the stress-strain curve obtained from a tensile test is used to represent the equivalent stress - equivalent strain curve for the material in the disk. As plastic flow progresses in the disk, the equivalent stresses and strains are computed in such a manner that they lie on the curve obtained from the tensile test. In the range of temperatures investigated, the stresses and strains in the solid, parallel-sided disks were highest at the center. For the cases in which instability does not occur, a disk failure should occur when the equivalent stress and strain at the center of the disk reach the end of the tensile stress-strain curve (which was the point at which the tensile specimen failed).

The maximum strains obtained at fracture under various conditions of biaxial loadings have been found in references 11 to 14 to be somewhat less than those which would be predicted from the results of tensile tests on the same material. Under biaxial conditions, it has been well established that ductilities decrease as the ratio of principal stresses S_2/S_1 increases from 0 for a tensile test to $S_2/S_1 = 1/2$, and possibly the ductility may continue to decrease as $S_2/S_1 \rightarrow 1$, but not much is known about biaxialities greater than $1/2$. The scatter in the results of various investigators seems to be too great to determine a definite value of loss in ductility for each condition of biaxiality.

In a solid disk the ratio of the radial and tangential stresses at the center is unity. Because materials lose ductility under biaxial loading, a solid, parallel-sided disk can be expected to fail with an equivalent strain at the center less than the strain at fracture of a tensile specimen. When the method of reference 2 is applied to a solid, parallel-sided disk, the calculated upper-limit failure speed is defined as the speed at which the equivalent stress and equivalent strain at the

center of the disk corresponds to the end point of the tensile-test stress-strain curve for the material, but because of the influence of biaxiality the disk is not able to reach this speed. The compilation of experimental data comparing actual burst speeds with calculated upper-limit failure speeds provides a basis for estimating failure speeds from calculations.

In figures 7 and 12 the theoretical change-in-diameter curves were extended beyond the last point obtained by measuring the test disk and were terminated at speeds corresponding to the calculated upper-limit failure speed. In figure 7 the experimental burst speed for the disk on which the change-in-diameter measurements were made is shown by the dotted line instead of a data point since it was not possible to determine the diameter of the disk at the instant before failure occurred.

It is conceivable that the center of a solid, parallel-sided disk subjected to a temperature gradient may not be the point where failure originates. Extremely high rim temperatures could make the rim the weakest part of the disk. The ratio of the equivalent stress in the disk at the calculated upper-limit failure speed to the fracture strength of a tensile specimen subjected to the same temperature as the material in the disk is shown in figure 19. The temperatures for curves B and C correspond to temperatures shown by curves B and C in figure 3. The material in the disk should fail at any point where the ratio of equivalent stress to fracture strength becomes unity in figure 19. For the range of temperatures in this investigation, the theoretical results show that failure originates in the center of the disk.

Relative Importance of Tensile Properties and Thermal Expansion

Theoretical results. - In comparing the results for room-temperature disks with those subjected to temperature gradients, there are two factors which operate to reduce the burst speed. If the disk is at a high but uniform temperature, no stresses are set up as the result of thermal expansion; however, the tensile properties of the material are lower than the room-temperature tensile properties, and the disk will burst at a correspondingly reduced speed. A disk subjected to a low center temperature and a high rim temperature has thermal stresses set up as the result of nonuniform expansion, and the rim material also suffers from a low tensile strength.

In order to evaluate the relative importance in the reduction of the burst speed, of the loss of tensile strength and of the stresses set up by the nonuniform thermal expansion, calculations were made under several assumptions. The assumptions and the results of the calculations are shown in table I.

The stress distributions at the calculated upper-limit failure speeds corresponding to the conditions of table I are shown in figure 20. In figure 20 the curves which show the importance of thermal expansion (condition 3), are nearly the same as the room-temperature curves, and the loss in calculated upper-limit failure speed shown in table I was only 300 rpm. The curves of the actual temperature-gradient conditions (condition 2) and the importance of material properties (condition 4) are very close together. The reduction below the room-temperature value of 46,200 rpm in calculated upper-limit failure speed for condition 2 was 1700 rpm and the reduction for condition 4 was 1400 rpm. Table I and figure 20 indicate that most of the loss in the calculated upper-limit failure speed in a disk with a high rim temperature and a large temperature gradient results from the loss in tensile properties of the material and not from the thermal stresses and strains set up in the disk.

The small effect of thermal expansion as just discussed is explained as follows:

For the 150° F center, 1440° F rim (curve B in fig. 3), the radial and tangential conventional strains at the center were 0.115 in./in. and the tangential strain at the rim was 0.048 in./in. at the calculated upper-limit failure speed. If the disk is not rotating and if the rim of the disk is permitted to expand freely, the rim will expand only 0.011 in./in. with a 1290° F temperature rise (1440-150=1290° F), and this is only about one-fourth the theoretical expansion in the rim that would occur under rotation and thermal gradient. With a temperature difference as large as 1290° F between the rim and the center, the strains resulting from thermal expansion are rather small when compared with the amount of plastic flow which is present at the calculated upper-limit failure speed for a disk of ductile material. Relatively small strains resulting from the nonuniform thermal expansion can produce only minor changes in the stress level in the disk or small reductions in the calculated upper-limit failure speed because the slope of the tensile specimen stress-strain curve is small in this region.

Experimental results. - The abscissa in figure 21 shows the temperature difference between the center and rim. The temperature-distribution curves corresponding to these temperature differences are presented in figure 3. The burst-speed points are the average of the burst speeds of a number of disks. The number of disks used to determine the average is shown in table II. At a temperature difference of 790° F in figure 21 a double point is shown. The lower point was based on the fact that a disk which was run under the 790° F temperature-difference conditions at 43,000 rpm did not burst. The upper point was based on the results presented in table II and the method of determining this point is presented in the discussion of table II in a following section.

The room-temperature point, the 790° F temperature-difference point, and the 1290° F temperature-difference point indicate a slight downward trend in burst speed with increasing temperature difference between the rim and center. These three points represent disk-center temperatures near room temperature, while the second point (520° F temperature difference) had a center temperature of 900° F and it does not follow the trend shown by the other three points.

Curve C of figure 3 shows the temperature distribution for the disks represented by the diamond data point (520° F temperature difference) in figure 21. With the exception of a very small part of the rim, the temperatures of curve C are much higher than those for curves A and B. In the preceding section on the theoretical importance of tensile properties and thermal expansion, the results indicated that the loss in tensile properties due to high temperatures was a very important factor in reducing the burst speed. Accordingly, the loss of material strength with temperature is concluded to be the reason why the second point of figure 21 lies below the line established by the other points.

In parallel-sided disks of a ductile material subjected to high rim temperatures and low center temperatures, the theoretical results showed that the loss in strength of the disk material caused most of the loss in burst speed and that the nonuniform thermal expansion contributed very little to the loss in burst speed. Even in the case of theoretical calculations which neglect the effects of thermal expansion in disks with a cool center, the higher the rim temperatures, the lower will be the calculated upper-limit failure speed. The experimental results in figure 21 show a slight lowering of the burst speed with increasing rim temperatures, and this is in agreement with the theoretical considerations. The disk with the 900° F center temperature in figure 21 had a more pronounced lowering of the bursting speed, and this experimental result also supports the theoretical calculations on the importance of the loss of strength of the disk materials.

For a tapered disk with high rim temperatures and low center temperatures, the influence of thermal gradients on the burst speed (if the failure originates at the center of the disk) is expected to be less than the influence of thermal gradients on parallel-sided disks because the total forces that can be exerted on the central region by the relatively thin rim of a tapered disk would be less than the total forces that could be exerted by the relatively thicker rim of a parallel-sided disk.

Determination of Predicted Burst Speed

The difference between the calculated upper-limit failure speed and the observed experimental burst speed can be used as a basis for

estimating the amount of correction for loss in ductility due to biaxiality. Figure 22 shows the agreement between the calculated upper-limit failure speed and the experimental burst speed. The experimental points would lie on the 45° line if the observed speeds were equal to the calculated upper-limit failure speeds. The percentage difference between the calculated upper-limit failure speeds and the experimental burst speeds is presented in line 5 of table II. The difference varies from 3.0 percent to about 5.3 percent if the average of the values listed for column 2 is used.

In the column for the temperature conditions corresponding to curve A of figure 3, two values for the experimental burst speed are listed. No disks were burst under these conditions, and the range of burst speeds was estimated in the following manner. The 43,000 rpm speed was based on the fact that a disk which was run under these conditions at 43,000 rpm did not burst, and hence 43,000 represents a lower limit for the burst speed under the conditions of curve A. The items marked with superscript a were computed on the basis of the 43,000 rpm speed. The upper limit of 43,600 rpm for the experimental burst speed was estimated from the results presented for the other test conditions in table II. The percentage difference between the calculated upper-limit failure speed and the experimental burst speed, the percentage loss in experimental burst speed, and the percentage loss in the calculated upper-limit failure speed were used to estimate the upper limit for the experimental burst speed. The average of the values listed in the first, third, and fourth columns of line 5 is 4.17 percent, and on this basis the experimental burst speed would be 43,790 rpm. The values listed in columns 3 and 4 of line 6 average 1.2 percent less than the values in line 7, and on this basis the experimental burst speed would be 43,460 rpm. The items in table II marked with superscript b were computed on the basis of the average of 43,460 and 43,790 rpm (43,600 rpm).

The percentage loss due to the temperature distributions in calculated upper-limit failure speed and the percentage loss in experimental burst speed (lines 6 and 7 of table II) are in good agreement for the conditions of column 3. In column 4 the calculated loss in burst speed was somewhat more than the experimental value.

The difference between the calculated upper-limit failure speed and the experimental burst speed was attributed to effects of biaxiality as mentioned in the discussion of the disk-failure process and to experimental errors. It was believed that experimental errors contributed very little to this difference. The calculated upper-limit failure speed in table II was from 3 to about 5.3 percent higher than the experimental burst speed. Results obtained by the method of reference 2 for room-temperature conditions in calculations prior to this investigation indicated that the calculated upper-limit failure speed should be reduced about 2 to 5 percent to predict the burst speed and these results are confirmed by the present investigation.

For the general case, a predicted burst speed could be obtained by reducing the calculated upper-limit failure speed by 4 percent. This predicted burst speed should then agree with the experimental burst speed within about +2 percent if the tensile specimen stress-strain curves are known accurately and if the disks are of high-quality material.

SUMMARY OF RESULTS

The 10-inch-diameter parallel-sided disks used in this investigation were subjected to short-time deformation and burst tests with center temperatures from 70° to 900° F and rim temperatures from 70° to 1440° F. The ductility was 19.4 percent (reduction in area) for a tensile specimen taken from the disk center, which was the point where failure originated. The following results were obtained:

1. All the results which were predicted by the theoretical calculations about the influence of temperature gradients on the behavior of disks were confirmed by the experimental observations over a wide range of conditions.

2. The curves of the theoretical change-in-diameter plotted against speed agreed with the experimental results in the range for which measurements were made (from the beginning of plastic flow to a speed 2.1 percent below the burst speed of the test disks). The theoretical strain distributions agreed with the plastic strain measurements.

3. Plastic flow occurred at a lower speed in an experimental disk subjected to thermal stresses than in a disk subjected to no thermal stresses, and the experimental results indicated that plastic flow started when the sum of the thermal and centrifugal stresses was equal to the yield point of the material.

4. The amount of plastic flow during the early stages of yielding was greater for a disk subjected to thermal stresses than for a disk subjected to no thermal stresses.

5. The temperature-gradient conditions produced little reduction in burst speed. The loss in burst speed for the experimental disk with the greatest temperature difference between the rim and center was 3.2 percent. The amount of reduction that did occur was dependent on the magnitude of the temperature difference between the rim and center of the disk.

6. For a ductile material the loss in tensile strength caused by increased temperature of the material had a greater effect in reducing the burst speed of the disk than the nonuniform expansion set up by the thermal gradient.

7. In order to predict burst speeds, the results of this investigation indicate that the calculated upper-limit failure speeds, which were based on the fracture point of the tensile specimen stress-strain curve, should be reduced by 4 percent to account for the loss in speed which was attributed to biaxiality. This predicted burst speed should then agree with the experimental burst speed within about ± 2 percent if the tensile-specimen stress-strain curves are known accurately for disks of high-quality material.

Lewis Flight Propulsion Laboratory
National Advisory Committee for Aeronautics
Cleveland, Ohio, July 10, 1952

APPENDIX - SYMBOLS

The following symbols are used in this report:

e_h	conventional thickness strain, in./in.
e_r	conventional radial strain, in./in.
e_t	conventional tangential strain, in./in.
$e_{r,n}$	conventional radial strains at the n^{th} point station and
$e_{r,n-1}$	the $(n-1)^{\text{th}}$ point station respectively, in./in.
r	radial distance, in.
S_1, S_2	principal stresses, lb/sq in.
u	change in radius, in.
du/dr	derivative with respect to r of the change in radius
ΔD	change in disk diameter, in.
ΔT	temperature increment above that temperature at which there is zero thermal stress, $^{\circ}\text{F}$
α	mean coefficient of thermal expansion between actual temperature and temperature at which there is zero thermal stress, in./in./ $^{\circ}\text{F}$
$\Delta_1, \Delta_2, \Delta_3$	logarithmic strains read from figure 17, in./in.
ϵ_h	logarithmic thickness strain, in./in., $\ln(1+e_h)$
ϵ_r	logarithmic radial strain, in./in., $\ln(1+e_r)$
ϵ_t	logarithmic tangential strain, in./in., $\ln(1+e_t)$
ρ	mass density, (lb)(sec ²)/in. ⁴
σ_e	equivalent stress, $\sqrt{\sigma_r^2 - \sigma_r \sigma_t + \sigma_t^2}$, lb/sq in.
σ_{fr}	fracture strength of a tensile specimen, lb/sq in.

σ_r radial stress, lb/sq in.
 σ_t tangential stress, lb/sq in.
 ω angular velocity of disk, radians/sec

Subscripts:

b station at rim of disk

$\left. \begin{array}{l} n \\ n-1 \end{array} \right\}$ stations

REFERENCES

1. Wilterdink, P. I.: Experimental Investigation of Rim Cracking in Disks Subjected to High Temperature Gradients. NACA RM E9F16, 1949.
2. Manson, S. S.: Analysis of Rotating Disks of Arbitrary Contour and Radial Temperature Distribution in the Region of Plastic Deformation. Paper presented at First U. S. Congress of Applied Mechanics (Chicago), June 11-16, 1951.
3. Tarr, Philip R.: Methods for Connection to Revolving Thermocouples. NACA RM E50J23a, 1951.
4. Anon.: Inconel "X" - A High Strength, High Temperature Alloy - Data and Information. Dev. and Res. Div., The International Nickel Co., Inc., rev., Jan. 1949.
5. Skidmore, Wallace E.: Bursting Tests of Rotating Disks Typical of Small Gas Turbine Design. Vol. VIII, no. 2, Proc. Soc. Exp. Stress Anal., Addison-Wesley Press, Inc. (Cambridge, Mass.), 1951.
6. Timosheko, S.: Theory of Elasticity. McGraw Hill Book Co., Inc., 1934, pp. 63-67.
7. Nadai, A.: Theory of Flow and Fracture of Solids. Vol. 1. McGraw-Hill Book Co., Inc., 1950, pp. 70, 73, 74.
8. Cross, Howard C., and Freeman, J. W.: Office of Naval Research and NACA Metallurgical Investigation of a Large Forged Disc of Inconel X Alloy. NACA TN 1770, 1949.
9. Dorn, J. E., Goldberg A., and Tietz, T. E.: The Effect of Thermal-Mechanical History on the Strain Hardening of Metals. Tech. Pub. No. 2445, Metals Technology, Sept. 1948.
10. Fraenkel, S. J.: Experimental Studies of Biaxially Stressed Mild Steel in the Plastic Range. Jour. Appl. Mech., vol. 15, no. 3, Sept. 1948, pp. 193-200.
11. Davis, H. E., and Parker, E. R.: Behavior of Steel under Biaxial Stress as Determined by Tests on Tubes. Jour. Appl. Mech., vol. 15, no. 3, Sept. 1948, pp. 201-215.
12. Sangdahl, G. S., Jr., Aul, E. L., and Sachs, G.: An Investigation of the Stress and Strain States Occurring in Bending Rectangular Bars. Vol. VI, no. 1, Proc. Exp. Stress Anal., Addison-Wesley Press, Inc. (Cambridge, Mass.), 1948, pp. 1-17.

13. Brown, W. F., Jr., and Sachs, George: Strength and Failure Characteristics of Thin Circular Membranes. Trans. A.S.M.E., vol. 70, no. 3, April 1948, pp. 241-251.
14. Brown, W. F., Jr., and Thompson, F. C.: Strength and Failure Characteristics of Metal Membranes in Circular Bulgings. Trans. A.S.M.E., vol. 71, no. 5, July 1949, pp. 575-585.

TABLE I - RELATIVE IMPORTANCE OF LOSS IN TENSILE STRENGTH AND THERMAL STRESSES



Conditions used for calculation		Calculated upper-limit failure speed (rpm)	Loss in calculated upper-limit failure speed (rpm)
Temperatures used to determine thermal expansion	Temperatures used to determine material properties		
1. ^a Room	Room	46,200	0
2. ^a 150°, 1440° F (curve B of fig. 3)	150°, 1440° F (curve B of fig. 3)	44,500	1700
3. ^b 150°, 1440° F (curve B of fig. 3)	Room	45,900	300
4. ^c Thermal expansion = 0	150°, 1440° F (curve B of fig. 3)	44,800	1400

^a These conditions correspond to those imposed on the experimental disks.

^b Effect of thermal expansion considered, but effect of loss in tensile strength was neglected because room-temperature material properties were assumed.

^c Effect of loss in tensile strength considered, but effect of thermal expansion was neglected.

TABLE II - SUMMARY OF RESULTS OF TEMPERATURE-GRADIENT DISK BURST SPEEDS

	Room temperature	Curve A of figure 3	Curve B of figure 3	Curve C of figure 3
1. Temperature condition, center rim		90°, 880° F	150°, 1440° F	900°, 1420° F
2. Experimental burst speed, rpm	43,900	43,000 ^a to 43,600 ^b	42,500	41,500
3. Number of disks averaged to obtain burst speed	6	0	3	2
4. Calculated upper-limit failure speed, rpm	46,200	45,700	44,500	42,800
5. Difference in speed, calculated upper-limit failure speed - experimental burst speed, percent	5.0	4.6 ^b to 5.9 ^a	4.5	3.0
6. Loss in experimental burst speed, percent	0	0.7 ^b to 2.0 ^a	3.2	5.5
7. Loss in calculated upper-limit failure speed, percent	0	1.1	3.7	7.4

^aLower limit was based on disk spun at 43,000 rpm without bursting.

^bUpper limit was estimated (see section entitled "Determination of Predicted Burst Speed").



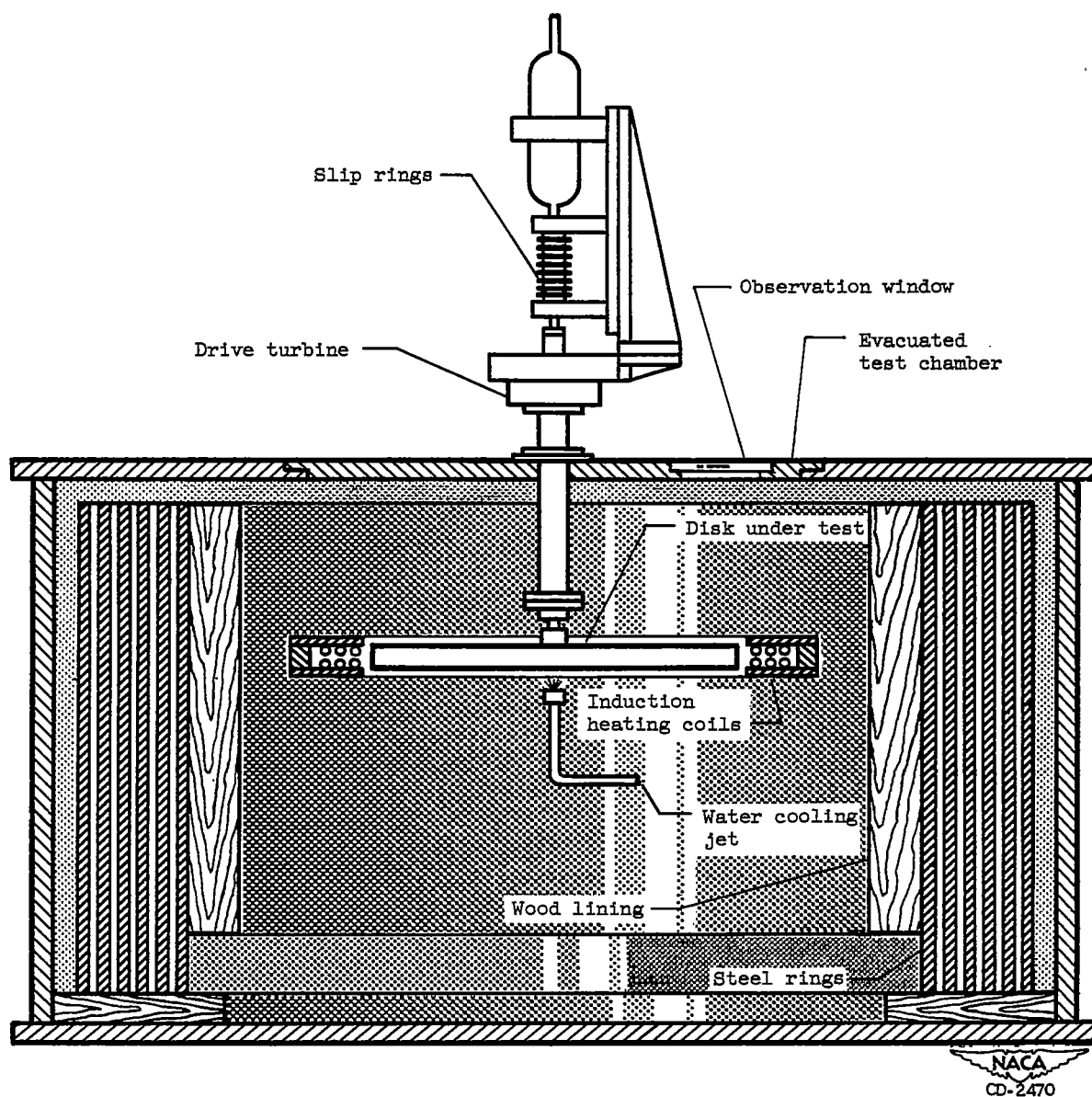


Figure 1. - Spin pit.

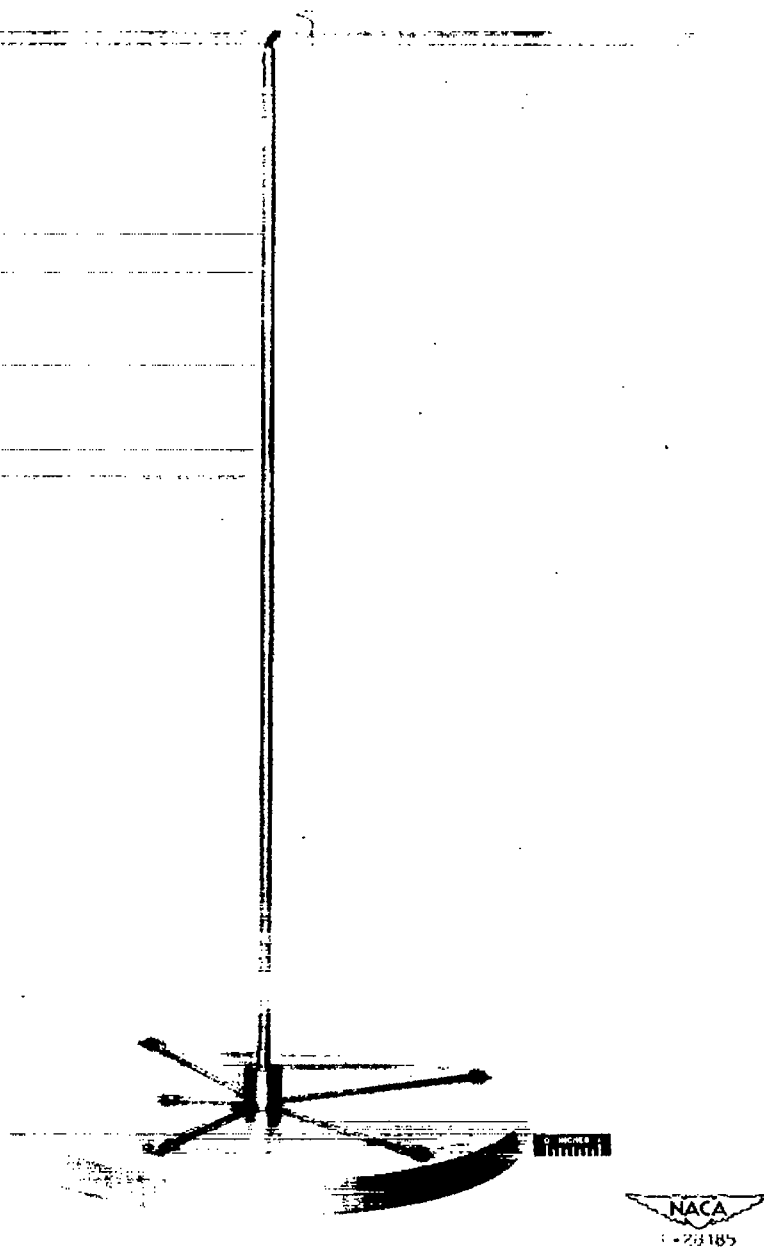


Figure 2. - Disk with thermocouples installed.

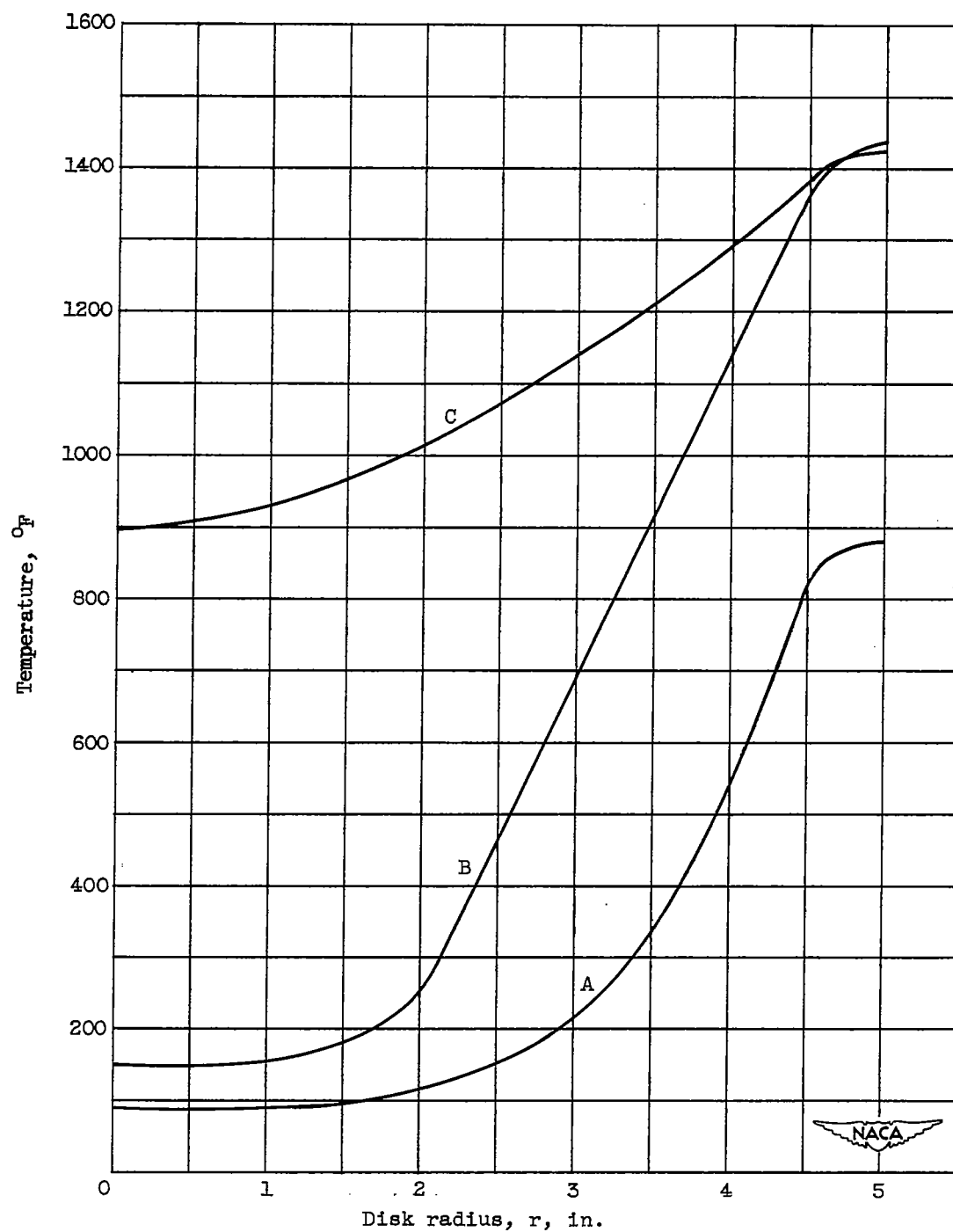


Figure 3. - Experimentally determined temperature distributions.

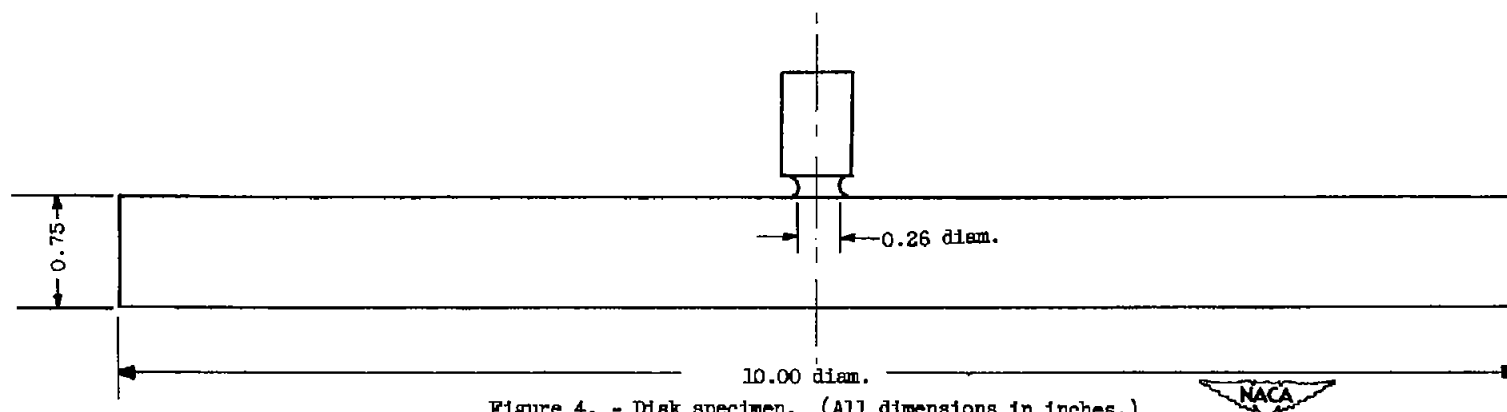


Figure 4. - Disk specimen. (All dimensions in inches.)



Figure 5. - Location of strain measurement stations.
(All dimensions in inches.)

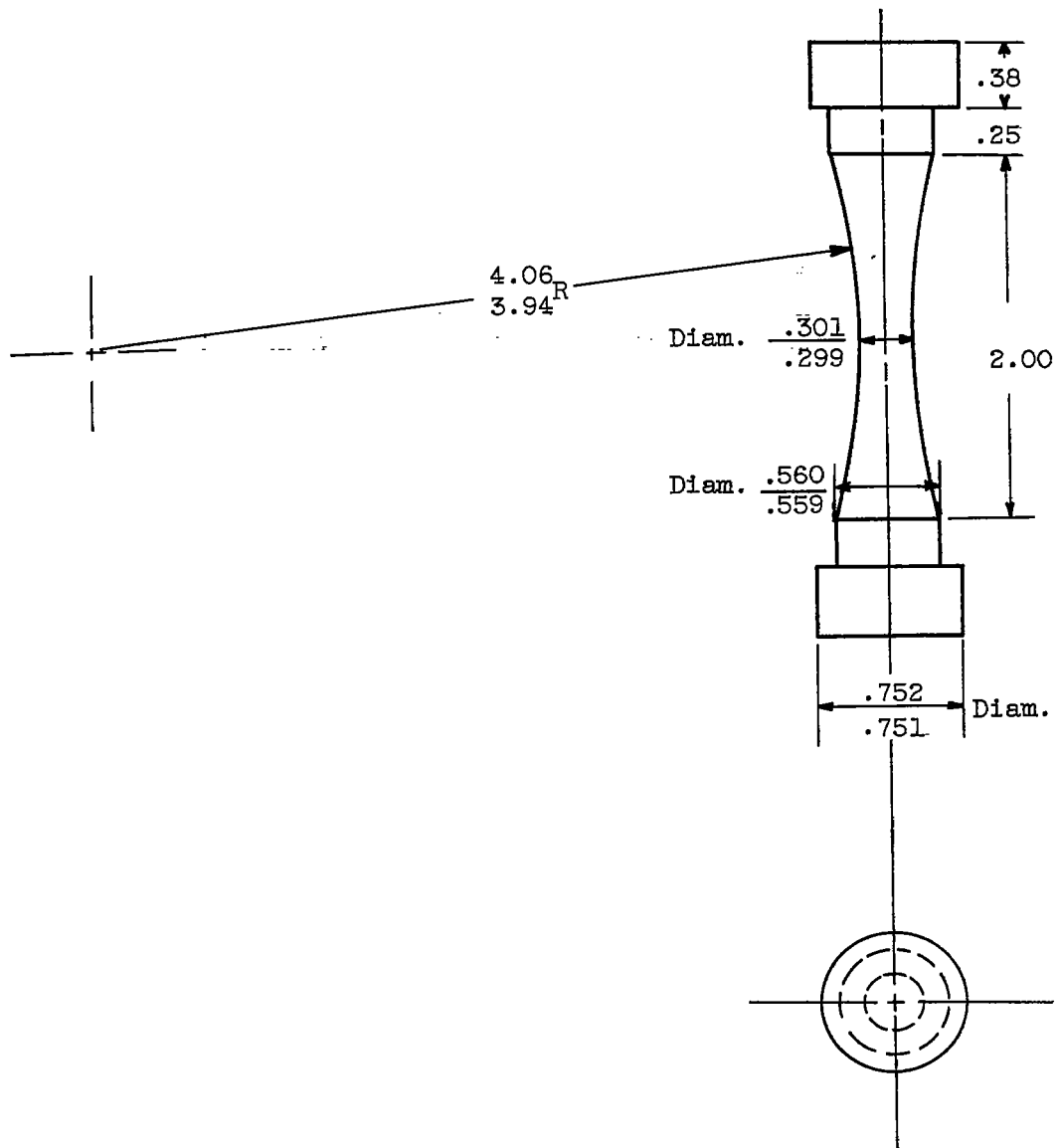


Figure 6. - Tensile specimen. (All dimensions in inches.)



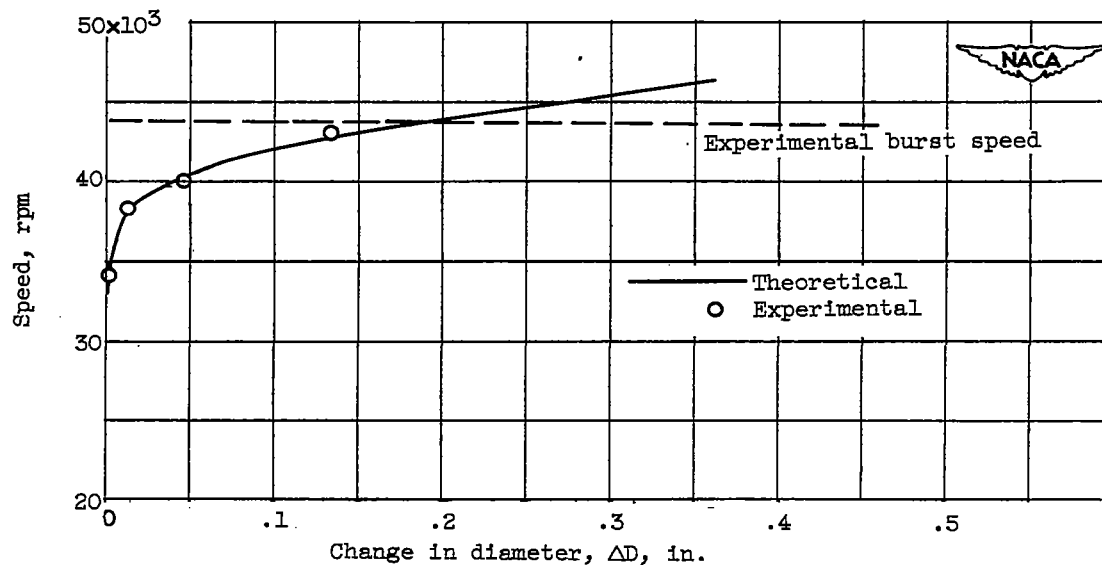


Figure 7. - Permanent change in diameter for disk tested at room temperature.

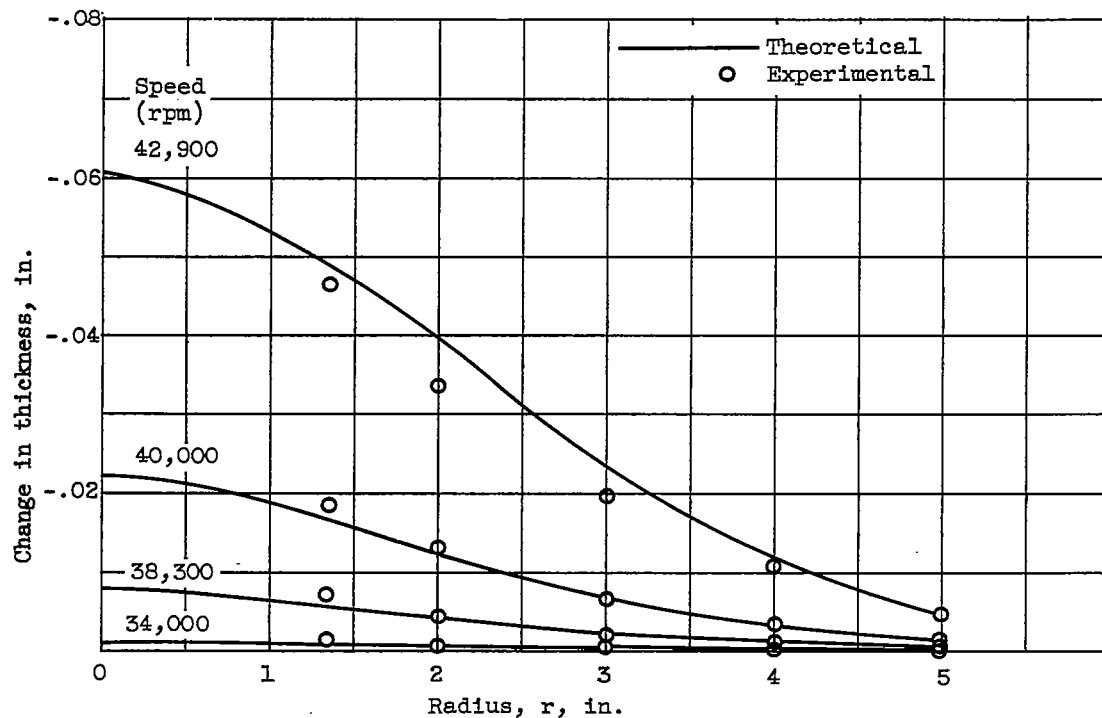


Figure 8. - Permanent change in thickness for disk tested at room temperature.

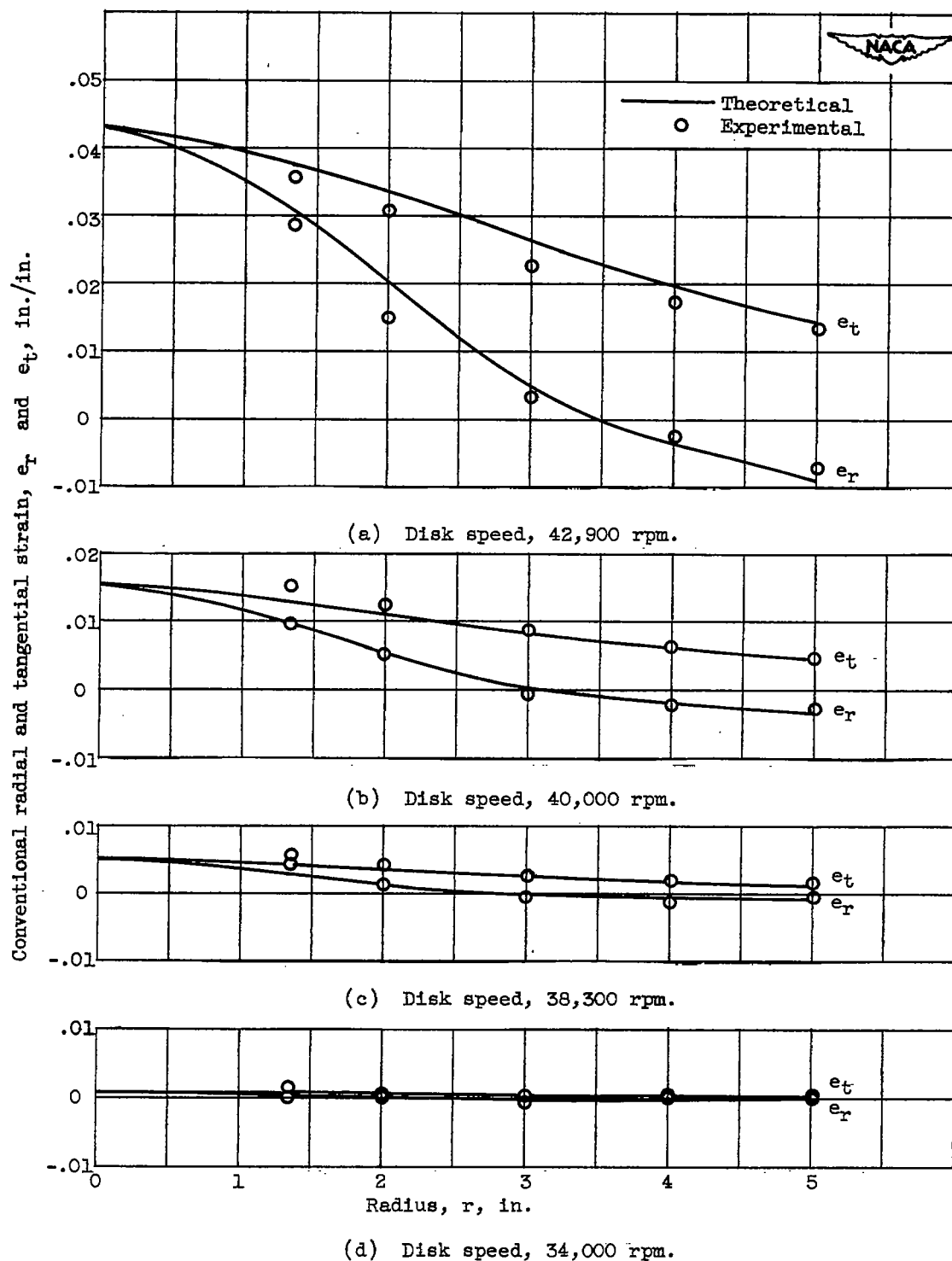


Figure 9. - Permanent conventional strains for disk tested at room temperature.

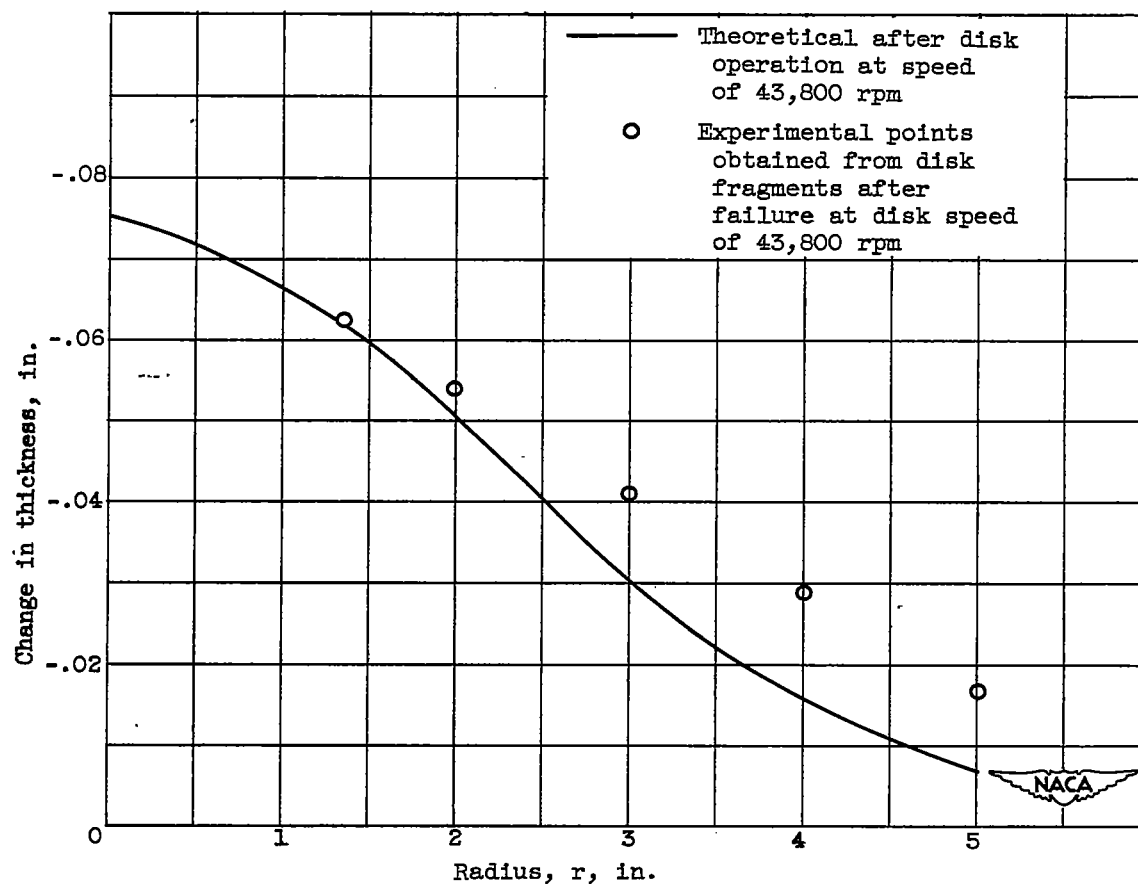


Figure 10. - Permanent change in thickness for disk tested at room temperature and 43,800 rpm.

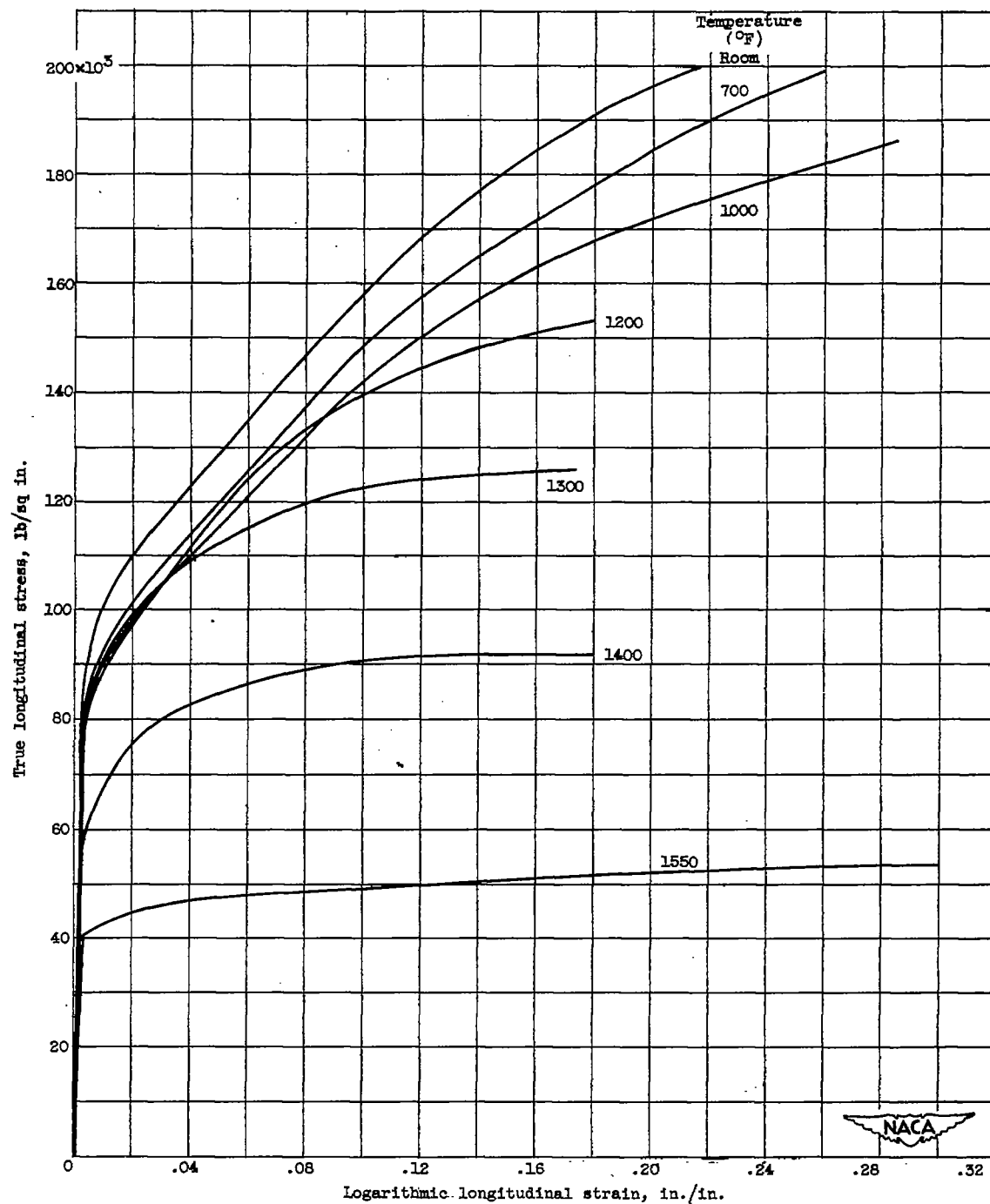


Figure 11. - Stress-strain data for Inconel X.

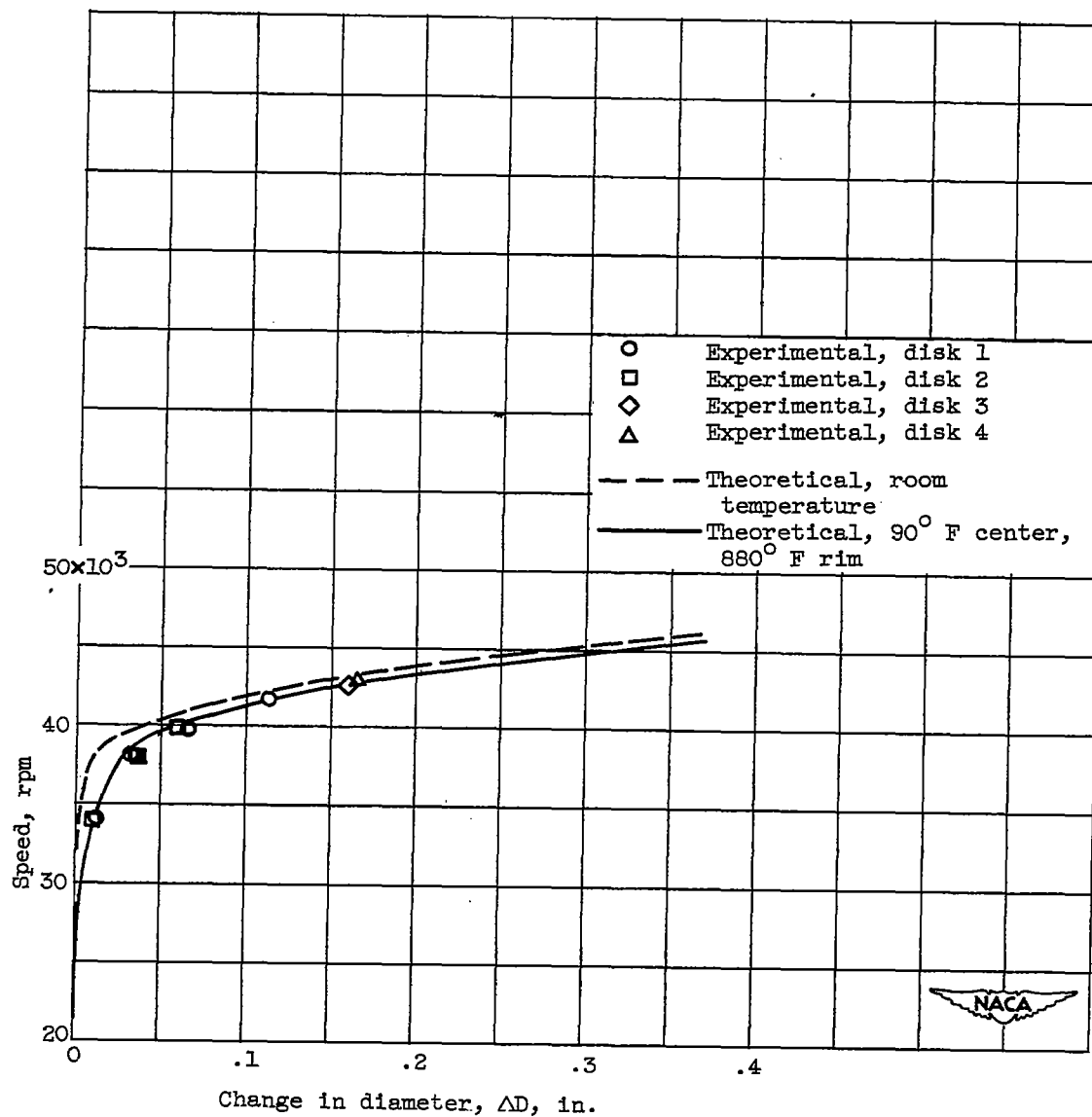


Figure 12. - Permanent change in diameter for disks tested with a 90° F center, 880° F rim and a disk tested at room temperature.

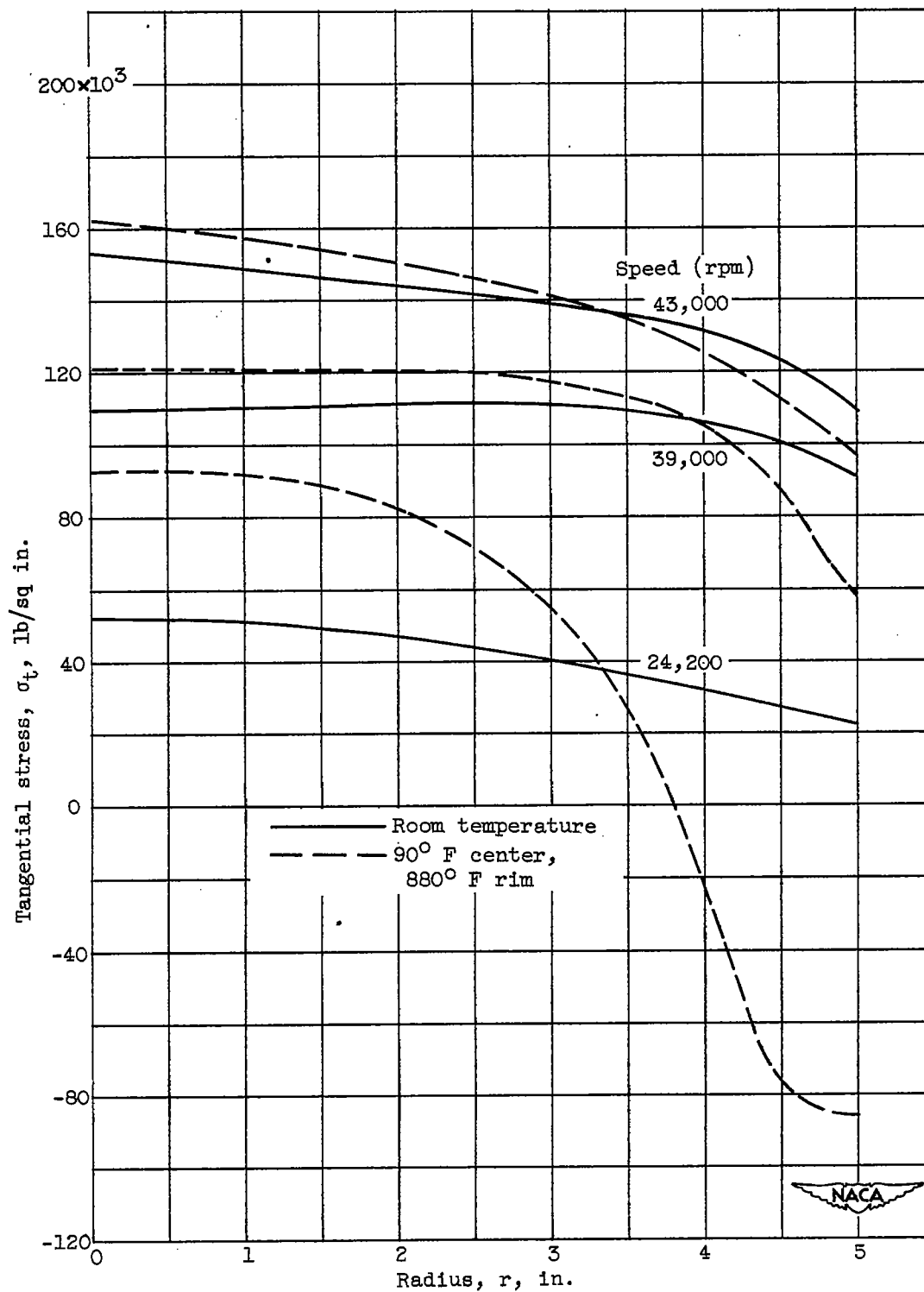


Figure 13. - Tangential stress distribution.

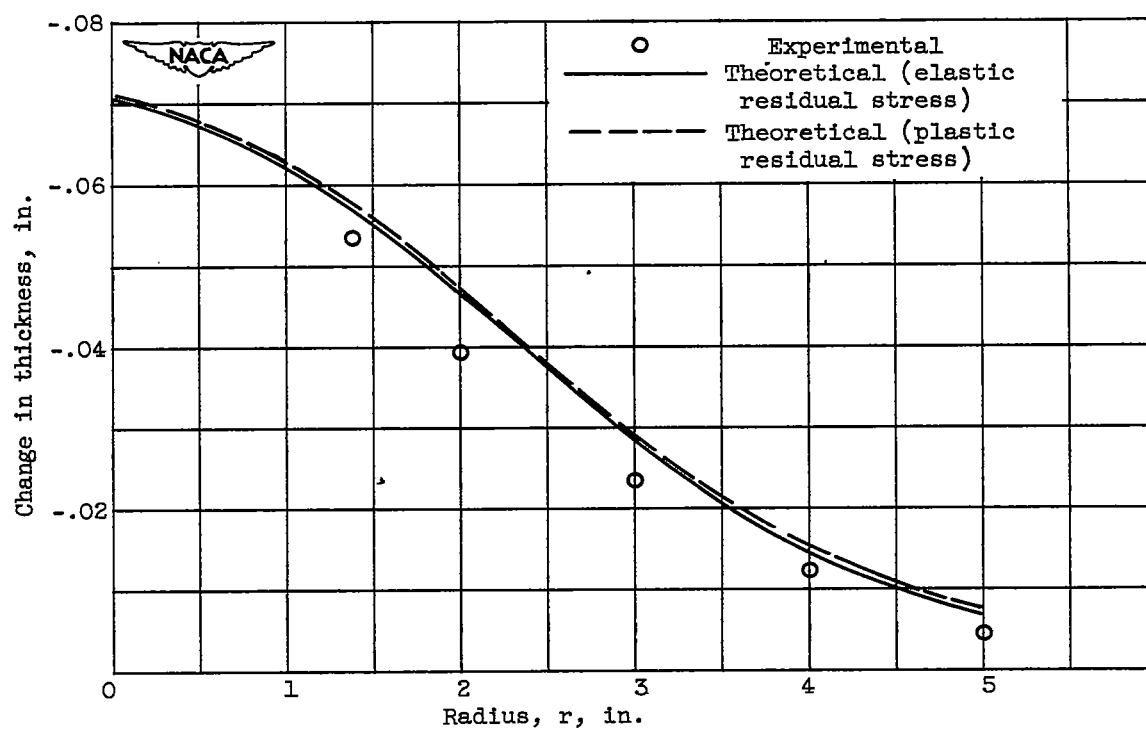


Figure 14. - Permanent change in thickness for disk tested with a 90° F center, 880° F rim at 43,000 rpm.

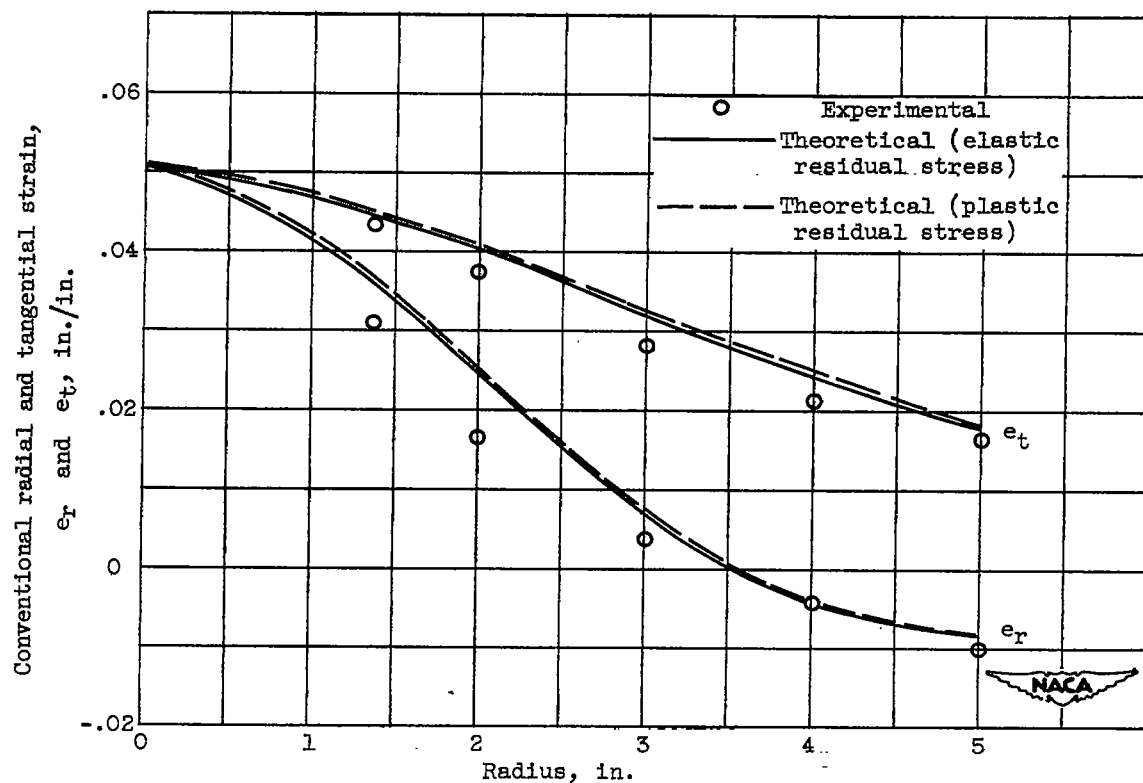
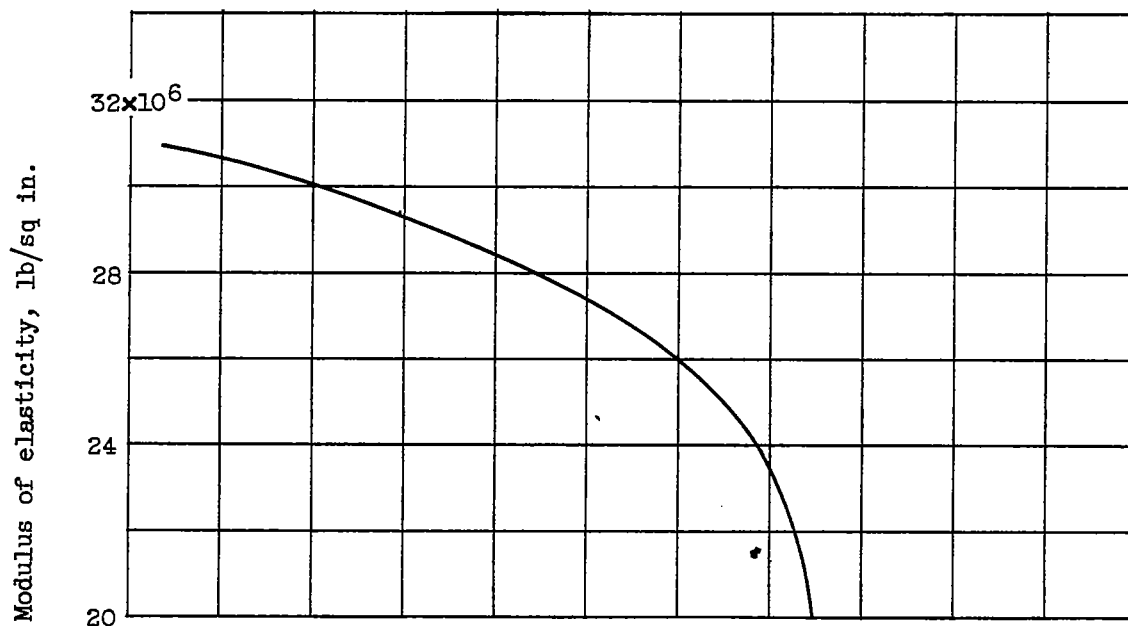
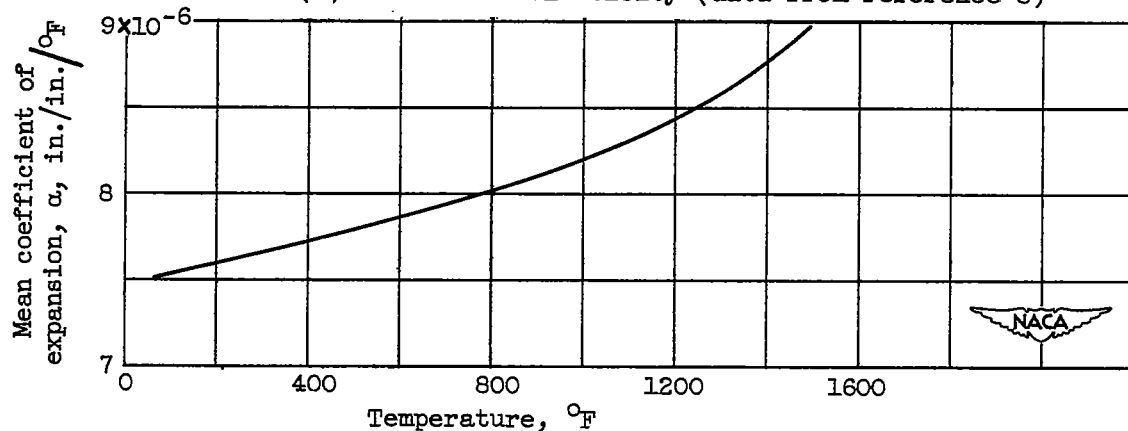


Figure 15. - Permanent conventional strains for disk tested with a 90° F center, 880° F rim at 43,000 rpm.



(a) Modulus of elasticity (data from reference 8)



(b) Mean coefficient of expansion (data from reference 4).

Figure 16. - Properties of Inconel X.

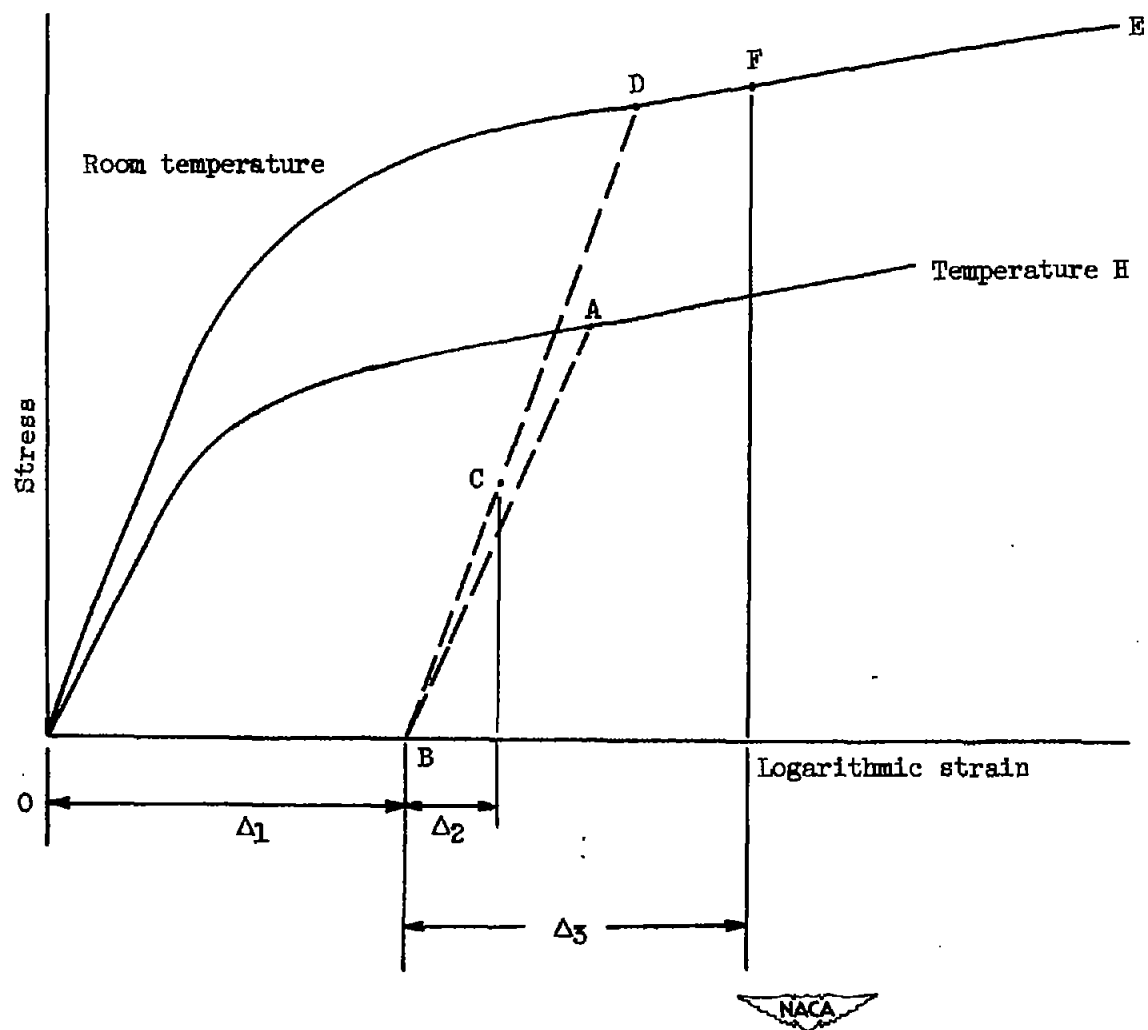


Figure 17. - Illustration of the use of stress-strain curves.

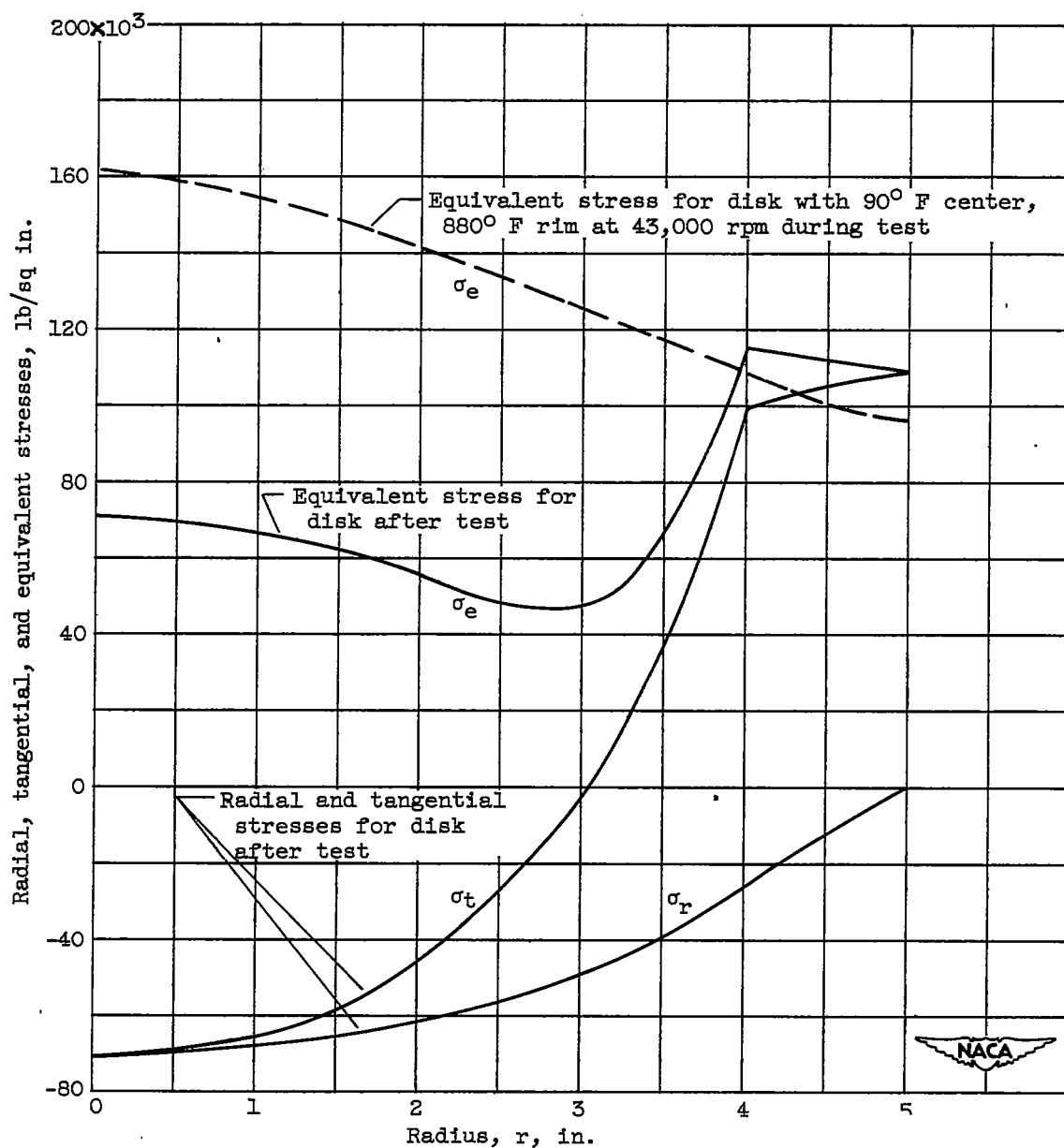


Figure 18. - Radial, tangential, and equivalent stress for disk tested with a 90° center, 880° F rim at 43,000 rpm.

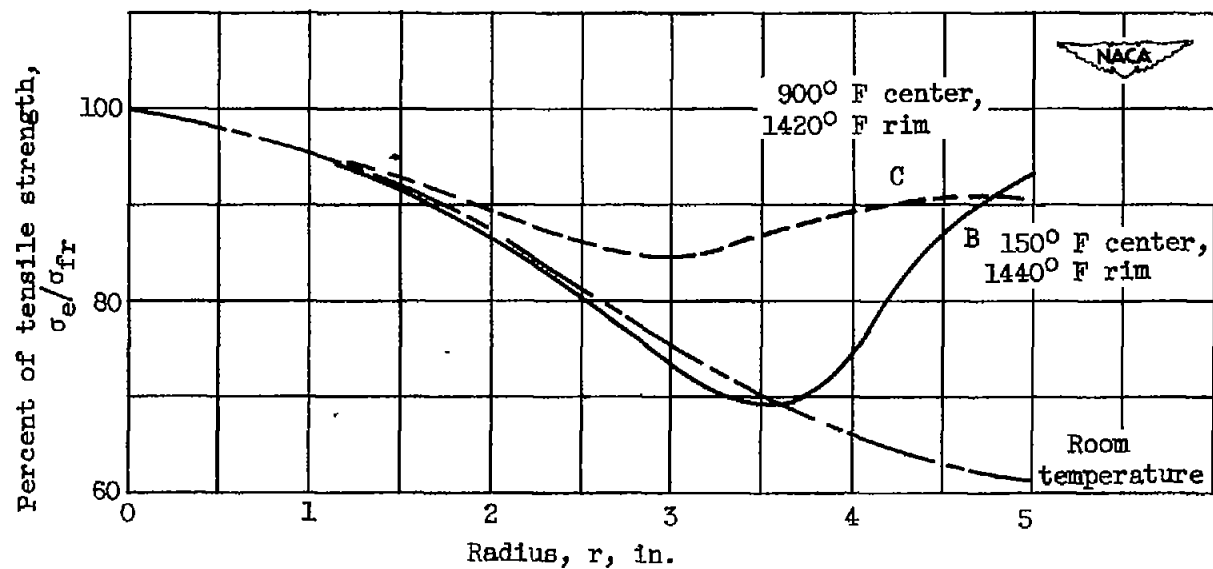


Figure 19. - Influence of temperature distribution on the ratio of equivalent stress at the calculated upper-limit failure speed to fracture strength.

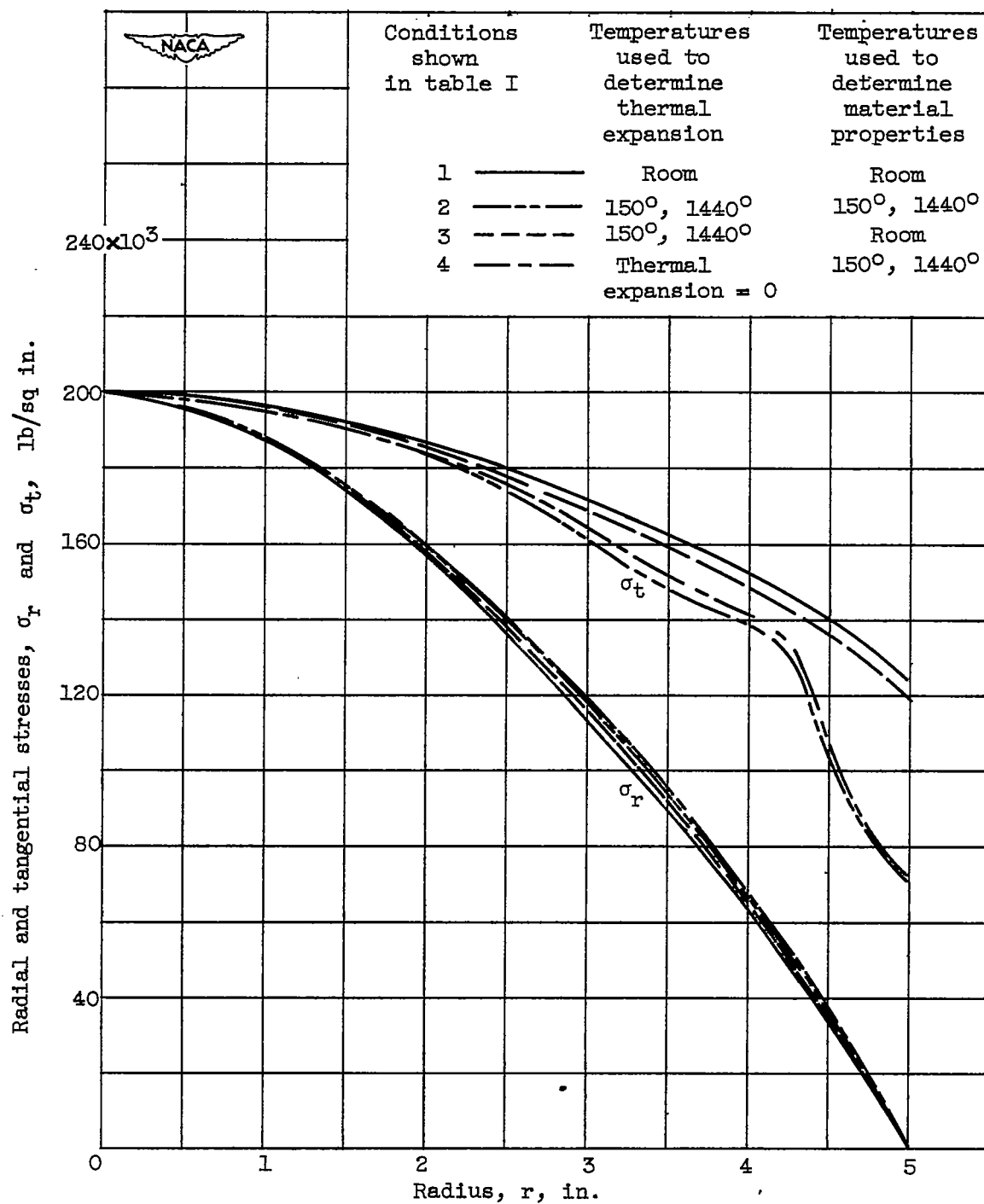


Figure 20. - Stresses at calculated upper-limit failure speed.

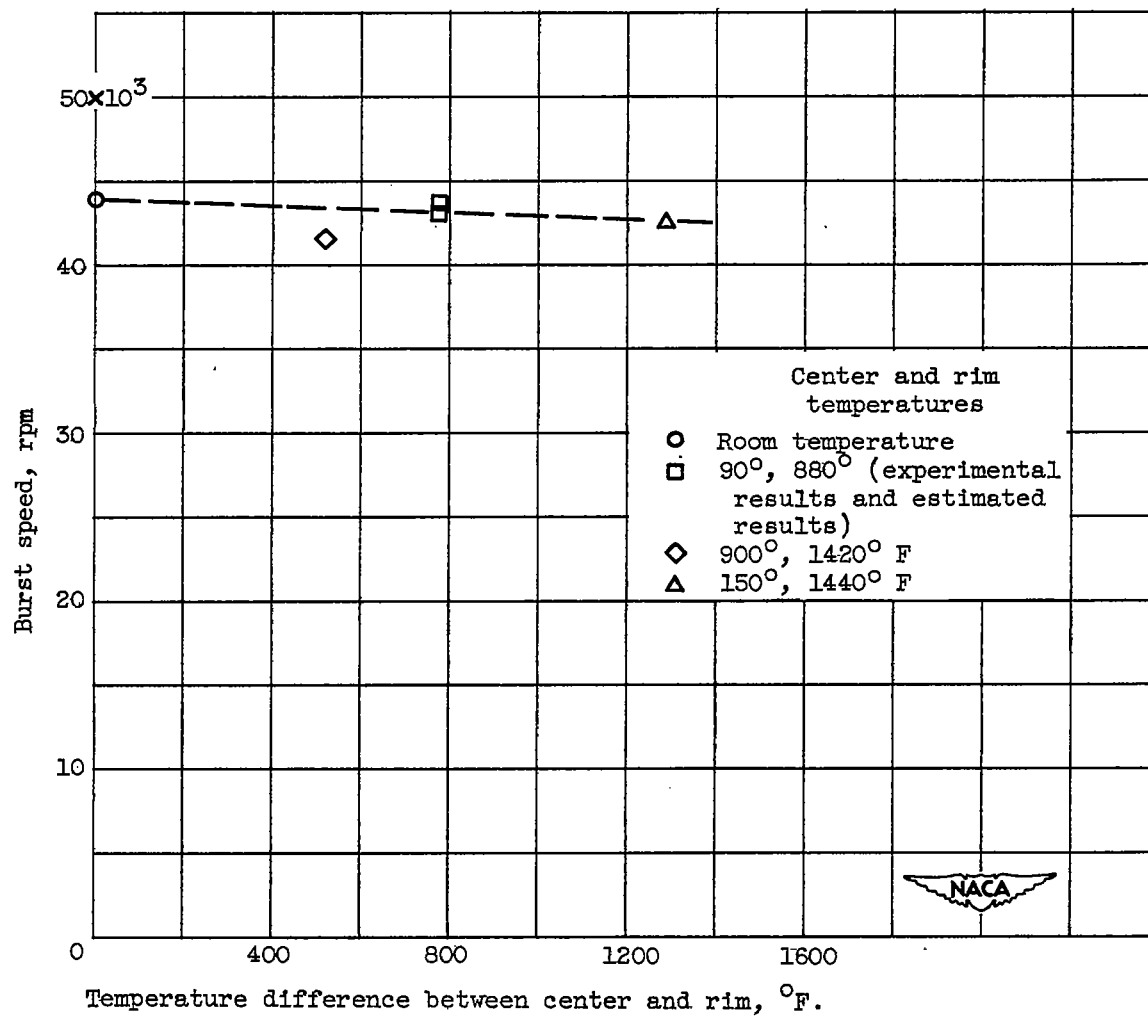


Figure 21. - Influence of temperature gradient on experimental burst speed.

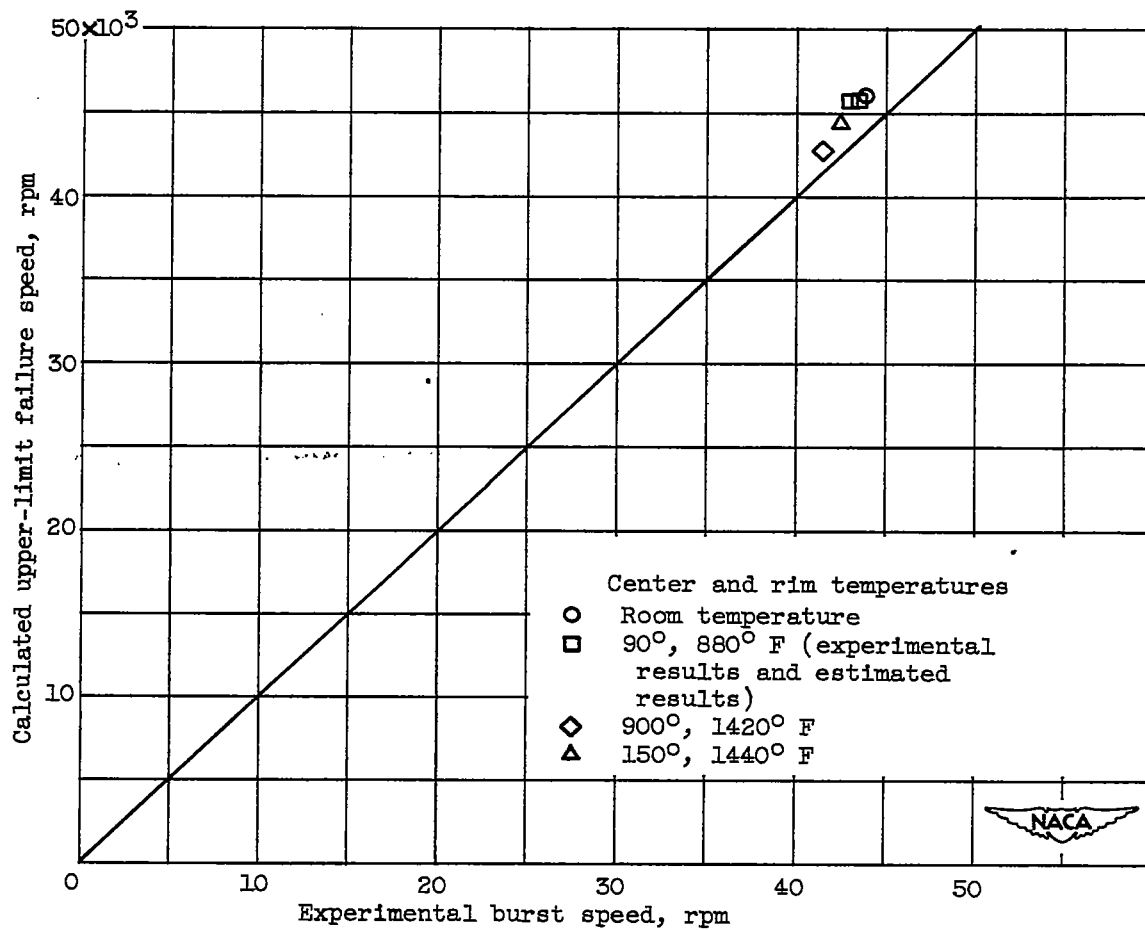


Figure 22. - Relation between calculated upper-limit failure speed and experimental burst speed.